****** in press, Geosphere ******

Revised after journal review
November 3, 2008

The Saddle Mountain Fault Deformation Zone, Olympic Peninsula, Washington: Western Boundary of the Seattle Uplift

Richard J. Blakely[1], Brian L. Sherrod[2], Jonathan F. Hughes[2*], Megan L. Anderson[3], Ray E. Wells[1], and Craig S. Weaver[2]

[1]U.S. Geological Survey, 345 Middlefield Rd, Menlo Park, CA 94025, USA

[2]U.S. Geological Survey, University of Washington, Seattle, WA 98195, USA

[3]Geology Department, Colorado College, Colorado Springs, CO 80903, USA

ABSTRACT

The Saddle Mountain fault, first recognized in the early 1970s, is now well mapped in the Hoodsport area on the basis of lidar surveys, aerial photography, and trench excavations. Drowned trees and trench excavations demonstrate that the Saddle Mountain fault produced a M_W 6.5 to 7.0 earthquake 1000-1300 ka, arguably contemporaneous with the M_W 7.5 Seattle fault earthquake 1100 years ago and with a wide variety of other fault and landslide activity over a wide region of the Olympic Peninsula and Puget Lowland. This near synchroneity suggests that the Saddle Mountain and Seattle fault may be kinematically linked. Aeromagnetic anomalies and lidar topographic scarps define an en echelon sequence of faults along the southeastern Olympic Peninsula of Washington, all active in Holocene time. A detailed analysis of aeromagnetic data suggests that the Saddle Mountain fault extends at least 35 km, from 6 km southwest of Lake Cushman to the latitude of the Seattle fault. A magnetic survey of Price Lake using a nonmagnetic canoe illuminated two east-dipping reverse faults with 20 m of vertical offset at 30 m depth associated with 2 to 4 m of vertical displacement at the topographic surface. Analysis of regional aeromagnetic data indicates that the Seattle fault may extend westward across Hood Canal and into the Olympic Mountains, where it terminates near the northward terminus of the Saddle Mountain fault. The en echelon

* Now at Department of Geography, University of the Fraser Valley, Abbotsford, BC, V2S 7M8, Canada

alignment of the Saddle Mountain and nearby Frigid Creek and Canyon River faults, all active in late Holocene time, reflects a >45-km-long zone of deformation that may accommodate the northward shortening of Puget Lowland crust inboard of the Olympic massif. In this view, the Seattle fault and Saddle Mountain deformation zone form the boundaries of the northward advancing Seattle uplift.

INTRODUCTION

Geophysical, lidar (light detection and ranging), and paleoseismic studies are uncovering a rich history of Holocene earthquake activity in the Puget Lowland. Paleomagnetic studies, GPS measurements, and geologic arguments indicate that the Oregon forearc is rotating clockwise and moving northward with respect to cratonic North America at rates of about 1°/m.y. and 6-8 mm/yr, respectively (Wells et al., 1998; Mazzotti et al., 2002; McCaffrey et al., 2007). In the Puget Lowland, the resulting north-south compression causes 4.4 ±0.3 mm/yr of permanent shortening (Mazotti et al., 2002; McCaffrey et al., 2007), accommodated in part by a series of east- and southeast-striking faults that cross the Lowland (Figure 1). Although recurrence intervals and earthquake magnitudes are uncertain in most cases, recent surface-rupturing earthquakes have occurred on many of these faults, including the Utsulady Point fault (Johnson et al., 2004b), the southern Whidbey Island fault (Johnson, et al., 1996; Kelsey et al., 2004; Sherrod et al., 2008), the Seattle fault (Johnson et al., 1994; Pratt et al., 1997; Blakely et al., 2002; Nelson et al., 2003), the Tacoma fault (Johnson et al., 2004a; Sherrod et al., 2004), and the Olympia fault (Sherrod, 2001). The most recent large (M_W7.5) crustal earthquake in the Puget Lowland occurred on the Seattle fault approximately 1100 ka, lifting the hanging wall of the Seattle fault 7 m, causing landslides, and generating a local tsunami (Bucknam et al., 1992; Atwater and Moore, 1992; Nelson et al., 2003; Sherrod, 2001; Karlin and Abella, 1996; ten Brink et al., 2006).

Active faults are also well known in the Olympic Peninsula west of the Puget Lowland (e.g., Carson, 1973; Nelson et al., 2007). Perhaps best known of these is the Saddle Mountain fault, with a surface trace initially reported to extend about 8 km (Figures 2 and 3; Carson, 1973; Wilson, 1975; Hughes, 2005; Witter and Givler, 2008).

Several issues warrant a closer look at the Saddle Mountain fault and surrounding tectonic framework. First, the Saddle Mountain fault generated a M 6.5 to 7.0 earthquake 1000-1300 ka (Hughes, 2005), within the same century or two as the M_W 7.5 Seattle fault earthquake. While modern dating techniques have insufficient resolution to determine if these two events were synchronous, it is important in assessing future earthquakes to understand any structural connections between the Saddle Mountain and Seattle faults. Second, although the surface expression of the Saddle Mountain fault was first reported to extend only about 8 km, geophysical evidence may help map the full extent of the fault in the subsurface, thus providing better estimates of its potential hazard. To help address these issues, we analyzed existing aeromagnetic and gravity data from the entire Olympic Peninsula and conducted ground-based magnetic surveys to characterize the Saddle Mountain fault in three dimensions. We also report on a paleoseismic trench investigation across one of the active faults along the southeast flank of the Olympic Mountains.

GEOLOGIC SETTING

The Saddle Mountain fault is located on the southeast flank of the Olympic Mountains (Figure 1), an accretionary complex consisting of two distinctive terranes. Highly deformed, pervasively sheared, and metamorphosed Eocene to Miocene sedimentary rocks form the core of the Olympic Peninsula. These core rocks are thrust under peripheral rocks of Eocene oceanic basalt and marine sediments along steeply dipping thrust faults (Figures 4 and 5; Cady, 1975; Tabor and Cady, 1978a, 1978b). Severe disruption of the eastern part of the core and a general westward decrease in age provide strong evidence that all of these rocks were emplaced by subduction processes (Tabor and Cady, 1978a). Initial accretion of the complex began as early as late Oligocene, followed by exhumation that started around 18 Ma and continues today at approximately uniform rates (Brandon et al., 1998). Uplift of the Olympic Mountains is domal in shape, with highest rates (>1 mm/y) near the center of the Olympic massif, tapering to less than 0.3 mm/y in the Saddle Mountain area (Brandon et al., 1998).

Peripheral rocks consist primarily of early to middle Eocene Crescent Formation basalts and associated volcanic and sedimentary rocks, an over-thickened volcanic assemblage of oceanic affinity and part of the Eocene Coast Range terrane extending from southern Oregon to Vancouver Island (Brown et al., 1960; Snavely and Wagner, 1963; Babcock et al., 1992). Tabor and Cady (1978a) considered the peripheral volcanic rocks to be a resistive bulwark against which subducting sediments were tilted, faulted, and sheared (Figure 5). In the southeastern Olympic Peninsula, peripheral volcanic rocks are up to 16 km thick, dip steeply eastward, and are overlain by Oligocene and younger sediments; farther east they are exposed in parts of the Seattle uplift and form part of the basement beneath the Seattle, Dewatto, and Tacoma basins (Figure 1; Tabor and Cady, 1978b; Brocher et al., 2004; Johnson et al., 2004a).

Along the eastern and southeastern margin of the Olympic Peninsula, Crescent Formation basalts consist of two important units: an upper member of basalt flows and mudflow breccia and a lower member of massive flows, pillow basalts, breccia, and minor intrusive rocks (Tabor and Cady, 1978b). The lower-member basalts are locally altered and metamorphosed to phrenite–pumpellyite and greenschist facies (Hirsch and Babcock, 2006) and commonly exhibit pillows and tube structures. Upper-member basalts are characterized by closely spaced joints and local columnar jointing. On the basis of geochemical arguments, Glassley (1974) concluded that lower-member basalts were created at a mid-ocean ridge in the early Eocene, subducted beneath similarly aged upper-member basalts, and then faulted upward into their present juxtaposition in Miocene time. Cady (1975), on the other hand, described the lower- and upper-member contact as a simple upward gradation, from a deep-water marine origin to a shallow-water marine and terrestrial origin – observations later confirmed by Hirsch and Babcock (2006).

The Saddle Mountain fault exhibits surface traces easily seen in aerial photography and lidar images (Figures 2 and 3). Carson (1973) first described scarps of the Saddle Mountain fault in detail, although there is anecdotal evidence that loggers recognized its topographic expression many years earlier. Wilson (1975) mapped the fault and recognized Pleistocene or younger deformation on three stands: the northeast-striking Saddle Mountain West and Saddle Mountain East faults and the northwest-

striking Dow Mountain fault. Witter and Givler (2008) noted a fourth fault striking northeast along the flank of Dow Mountain (Figures 2 and 3). Several other active faults with similar northeast strike are observed in the lidar data: the Frigid Creek fault about 2 km to the south (Figure 2; Haugerud and Sherrod, 2007; Witter and Givler, 2008) and the Canyon River fault about 27 km to the southwest (Walsh and Logan, 2007).

Lidar images and field examinations indicate that both the Saddle Mountain West and Saddle Mountain East faults exhibit southeast-side-up displacement, with scarps exceeding 8-m high in many places (Figure 3). Early trench excavations (Wilson, 1975; Wilson et al., 1979) confirmed that the scarps were created by reverse faults offsetting late Pleistocene glacial deposits and early Eocene Crescent Formation basalt. A recent trench excavated across the Saddle Mountain West fault (Witter and Givler, 2008) exposed evidence for two earthquakes, one occurring between 17 and 8.5 ka, and a second occurring after 1.7 ka. Total vertical offset for both earthquakes at this most recent trench site was about 1 m, although the 1.7-m scarp height suggests that only part of the deformational history was exposed in the trench. Lateral slip also may have been important in these earthquakes. Southwest-plunging striations observed on the hanging wall of the Saddle Mountain East fault plane indicate left-lateral movement (Wilson et al., 1979), while a basalt cobble lodged in till and split by a secondary fault suggests dextral displacement along the Saddle Mountain West fault (Witter and Givler, 2008). The northeast-striking Canyon River fault, 27 km to the southwest, shows clear evidence of oblique left-lateral slip in Holocene time (Walsh and Logan, 2007), suggesting that right-lateral slip along the Saddle Mountain West fault seen by Witter and Givler (2008) was a local phenomenon rather than a persistent kinematic feature of the region.

Carson (1973) first suggested that slip on the Saddle Mountain East fault dammed Price Lake (Figures 2 and 3) about 1100 years ago, drowning a forest that existed at the time. Hughes (2005) analyzed stumps beneath Price Lake and concluded that both the Saddle Mountain West and Saddle Mountain East faults ruptured between 1000 and 1300 years ago, possibly during the same earthquake. This earthquake may have caused as much as 4 m of vertical offset on the Saddle Mountain East fault and 2 m of offset on the Saddle Mountain West fault (Hughes, 2005) and probably generated the 1.7-m slip observed in the Saddle Mountain West fault trench (Witter and Givler, 2008). These

estimates agree with trench excavations made in the 1970's across the Saddle Mountain East and West scarps (Wilson, 1975; Wilson et al., 1979), which revealed 3.5 m and 1.8 m of reverse slip, respectively. The bracketed time of this earthquake (1000 to 1300 years ago) includes the time (1020-1050 years ago) of the M_W7.5 earthquake on the Seattle fault and corresponds temporally with a wide variety of other fault and landslide activity over a wide region of the Olympic Peninsula and Puget Lowland (Schuster et al., 1992; Logan et al., 1998; Haugerud et al., 2003; Walsh and Logan, 2007).

ANALYSIS OF REGIONAL GEOPHYSICAL DATA

Figure 6 shows gravity and magnetic anomalies of the eastern Olympic Peninsula and adjacent Puget Lowland. Magnetic anomalies are based on an aeromagnetic survey flown in 1997 by the U.S. Geological Survey (Blakely et al., 1999). Flight altitude was nominally 300 m over flat to moderate terrain, but significantly higher altitudes were necessary over river valleys and along the eastern margin of the Olympic Mountains. Most of the study area was flown along north-south flight lines spaced 400 m apart and along east-west tie lines spaced 8 km apart. Flight-line and tie-line spacings were doubled in the northwestern part of the study area, where the magnetic field is characterized by longer wavelengths. Gravity anomalies shown in Figure 6b are based on point measurements from the Pan-American Center for Earth and Environmental Studies (PACES) repository (http://paces.geo.utep.edu/home.shtml), supplemented with unpublished data (Thomas Wiley, written communication, 2008). Gravity anomalies have been reduced to isostatic residual gravity values in order to emphasize middle and upper crustal sources (Simpson et al., 1986). Gravity measurements are sparse in some areas, especially over Hood Canal and within inaccessible parts of the Olympic Mountains, but in most areas station density is adequate (at least one station per 25 km^2) to define regional-scale structures.

Low densities and magnetizations of sedimentary and metamorphic rocks of the core terrane produce subdued, low-amplitude gravity and magnetic anomalies. In contrast, relatively high densities and magnetizations of Crescent Formation rocks produce high amplitude anomalies over the peripheral terrane. Moreover, the upper and

lower members of Crescent Formation appear geophysically distinct. This is particularly evident south of latitude 48º45'N., where gravity anomalies (Figure 6b) are broadly associated with the entire exposure of Crescent Formation basalts, but high-amplitude magnetic anomalies (Figure 6a) primarily reflect only the upper-member basalts.

Magnetic susceptibility measurements made at Crescent Formation outcrops confirm this overall pattern (Figures 6a and 7; Table 1). In general, high susceptibilities are observed in regions with high-amplitude magnetic anomalies, which coincide with the mapped extent of upper-member basalts. Low susceptibilities and low-amplitude magnetic anomalies characterize the lower-member basalts. This relationship is particularly clear in the Saddle Mountain area (Figure 7), where all mean susceptibility values in the Price Lake and Dow Mountain area (upper-member basalts) exceed 18 x 10^{-3} SI (Systèms Internationale) units, whereas all mean values along Lake Cushman (lower-member basalts) fall below that value.

Figure 8 shows a cross-sectional model through the Saddle Mountain area based on forward simultaneous modeling of gravity and magnetic anomalies, constrained by geologic mapping (Tabor and Cady, 1978b). The model is consistent with low-density, weakly magnetic core rocks thrust beneath steeply dipping, sometimes overturned peripheral volcanic rocks. Peripheral volcanic rocks are modeled in Figure 8 with nearly uniform densities, whereas upper-member basalts required a magnetization four times greater than lower-member basalts, consistent with our susceptibility measurements (Table 1). The model assumes that magnetizations are entirely induced, a reasonable assumption based on poor paleomagnetic results from most of the main Crescent outcrops (C.S. Gromme, Myrl Beck, and David Engebretson, personal communication, 1975-1982).

CANOE MAGNETIC SURVEY

The Saddle Mountain East and West faults offset highly magnetic upper-member basalt, and both faults are included in our cross-sectional model through Price Lake (Figure 8). Price Lake itself afforded an excellent opportunity to investigate the magnetic characteristics of the Saddle Mountain fault at outcrop scale (Figure 9). The alpine

setting of this small lake is devoid of man-made objects that deleteriously affect ground-based magnetic surveys, and the obvious lack of tree cover facilitated accurate GPS navigation. Measurements were made with a nonmagnetic canoe, GPS navigation, and a cesium-vapor magnetometer system. A stationary proton-precession magnetometer was maintained at lake shore to subsequently correct for time-varying fields. We acquired 26 track lines over the entire lake at an average track-line spacing of 40 m and a total line-distance of 9 km. Fifteen track lines crossed the lakeward projection of the Saddle Mountain West lidar scarp, but the Saddle Mountain East scarp was unreachable by canoe. The canoe-magnetic survey illuminated a linear, north-northeast-trending magnetic trough, approximately 150 m wide and 1000 nT in amplitude, on strike with lidar scarps northeast and southwest of the lake (Figure 9).

A cross-sectional model of the Saddle Mountain West fault (Figure 10) based on the canoe magnetic survey is consistent with two distinct strands of the Saddle Mountain West fault. Both strands are modeled as southeast-side-up reverse faults that offset Pleistocene and Holocene deposits at the surface and Crescent Formation at >30 m depth. Although our modeled offsets of Crescent Formation project upward to lidar scarps observed at the surface, the offsets at depth have significantly larger displacements (>20 m) than implied by either topography (scarps as high as 8 m) or trench excavations (dip slip as much as 3.5 m; Wilson et al., 1979), suggesting a long history of Quaternary deformation.

TECTONIC FRAMEWORK, SOUTHEASTERN OLYMPIC PENINSULA

The canoe-based magnetic survey of Price Lake demonstrates that individual strands of the Saddle Mountain fault are reflected in magnetic anomalies. We now step back and examine aeromagnetic anomalies at a regional scale. Our interpretation of the eastern and southeastern Olympic Peninsula (Figure 11) employed a variety of both quantitative and qualitative analyses of magnetic and gravity data, but we relied primarily on a method recently described by Phillips et al. (2007): Magnetic anomalies (Figure 6a) were reduced to the pole, transformed to maximum horizontal gradients, and analyzed for mathematical curvature. This three-step methodology provides the locations of abrupt

lateral variations in crustal magnetization, shown as sinuous alignments of small black dots in Figure 11b.

Linear alignments of black dots in Figure 11b indicate the map projection of magnetic contacts, which have diverse explanations in our large study area. Some contacts represent faults, notably the contact between highly deformed core rocks thrust beneath Crescent Formation in peripheral rocks (Figure 11c, label CPF—core-peripheral fault). Other contacts are caused by lateral variations in lithology or geochemistry, such as the marked contrast in anomaly amplitudes over upper- and lower-members of the Crescent Formation south of latitude 48º45'N. Still others may reflect folding within Crescent Formation rocks, although none of our calculated magnetic contacts (Figure 11b) directly correlate with folds mapped by Tabor and Cady (1978b). Within the Crescent Formation, magnetic contacts may reflect lateral changes from normal to reverse magnetization, although metamorphism and alteration of these volcanic rocks has probably reduced significantly their primary remanent magnetization.

The contrast in anomaly amplitude between upper- and lower-member Crescent Formation south of latitude 48º45'N. was an expected result in view of magnetic susceptibilities exhibited by these rocks (Figures 6a and 7, Table 1). The contrast in magnetic properties reflects differences in lithologic characteristics and levels of tectonic deformation: Lower-member basalts are highly sheared and deformed and contain abundant pillows, whereas upper-member basalts are characterized by massive flows, local columnar jointing, sparse pillows, and less deformation. The contrast in magnetic properties may reflect primary formation of magnetic minerals, possibly due to contrasting local environments at the time of formation, submarine environments for lower-member basalts and subaerial for upper-member basalts. Alternatively, the weak magnetization of lower-member basalts may reflect secondary alteration of magnetic minerals, either caused directly by the deformational events responsible for the pervasive shearing seen in these rocks, or promoted subsequently by migration of low-temperature water through loosely consolidated pillow structures (e.g., Marshall and Cox, 1972). The contrast in magnetic properties ends rather abruptly at latitude 48º45'N.; north of this latitude lower-member basalts produce anomalies similar in amplitude to the upper-

member basalts. Subdued anomalies south of latitude 48º45'N. may reflect local metamorphism to greenschist facies.

Saddle Mountain, Frigid Creek, and Canyon River faults

A pronounced northeast-striking magnetic anomaly lies directly over Saddle and Dow Mountains (Figures 2, 11, and 12), possibly caused by combined southeast-side uplift along both the Saddle Mountain East and West faults. The northwest-facing gradient of this magnetic anomaly yields a well-defined magnetic contact corresponding closely with the swath of scarps seen in lidar data (Figure 12, label SMF). The magnetic contact extends southwestward 4 km from Price Lake to Lake Cushman (Figure 12b), where it coincides with the northeast-striking Cushman Valley fault (Carson and Wilson, 1974; see Figures 2b and 3b for location of Cushman Valley). Witter and Givler (2008) suggested that the Saddle Mountain and Cushman Valley faults are surface expressions of the same structure, and our observations support their interpretation. Moreover, the magnetic contact and lidar scarps suggest that the Saddle Mountain fault extends even farther to the southwest, to at least 6 km west of Lake Cushman (Figure 12). Southwest of this point, the magnetic contact steps southward before continuing on southwestward. Thus, the Saddle Mountain fault, as expressed by lidar scarps, extends a minimum of 15 km, from northeast of Price Lake to southwest of Lake Cushman, and magnetic anomalies suggest that the fault extends an additional 5 km southwestward (Figure 12). In a later section, we describe evidence for extending the Saddle Mountain fault northeastward, well beyond mapped lidar scarps.

The Frigid Creek fault (Figures 2 and 13) lies parallel to and 4 km south of the Saddle Mountain fault and exhibits a well-defined northwest-side-up scarp 2.7 m in height. A single trench excavated across the Frigid Creek scarp (Figure 14) revealed conformable strata consisting of oxidized sandy gravels, sandy loams, and sandy silts. Radiocarbon analyses by Lawrence Livermore National Laboratory showed that charcoal clasts collected from units 2 and 3 ranged in age from 5657-5476 cal yr B.P. (4850±40 14C yr B.P.) to 4513-4220 cal yr B.P. (3925±40 14C yr B.P.). A single clast of charcoal from unit 6 (part of the surface soil profile on the scarp) yielded an age of 526-319 cal yr

B.P. (415±40 14C yr B.P.). These strata resemble similar deposits observed throughout the southeast Olympic Mountains that consist of Holocene debris flows and soils developed on these debris flows that were buried by subsequent debris flows.

Beneath the scarp, the strata are offset by a normal master fault and several smaller antithetic normal faults, forming a small graben along the scarp. We interpret the offset strata as the result of movement along the normal master fault during an earthquake between 5657 and 319 cal yr B.P. The deformation is best interpreted as downward movement of two hanging-wall blocks (Blocks 2 and 3) relative to the footwall block (Block 1; Figure 14b). Downward movement and clockwise rotation of Block 2 formed a small graben adjacent to the scarp. Piercing points observed in the excavation show that 2.5 m of vertical separation can be accounted for in one event (93 percent of total 2.7 m scarp height). The unaccounted 0.2 m of scarp height suggests either an earlier and much smaller earthquake or differential erosion and deposition along the scarp after the earthquake.

We interpret the Frigid Creek fault as a bending-moment fault in the hanging wall of a large thrust sheet, or as a normal fault associated with a bend or step-over in a lateral fault system. The Frigid Creek fault lies astride a high-amplitude, sinuous magnetic anomaly (Figure 12) that we interpret as a fold in Crescent Formation. A magnetic contact is not observed directly along the Frigid Creek fault scarp, suggesting that the fault lies entirely above or roots into underlying Crescent Formation basalts. The Frigid Creek fault, with southeast side down, may be responding to subsidence of the Dewatto and Tacoma basins directly to the east and midway between the Olympia and Seattle uplifts (Figure 1b).

A narrow but pronounced magnetic anomaly (Figure 12, label OF—Olympia fault) and coincident gravity anomaly (Figure 6b) extend southeastward from Crescent Formation exposures in the Olympic Mountains to the southern edge of our study area, where the source of the anomaly is entirely concealed beneath Pleistocene glacial deposits. South of our study area, anomaly OF merges with the “Olympia structure” (Magsino et al., 2003), which juxtaposes near-surface Crescent Formation to the southwest against the Tacoma basin to the northeast (Figure 1). Coseismic subsidence

occurred along the Olympia structure approximately 1100 ka (Sherrod, 2001), and the linear nature of associated gravity and magnetic anomalies is highly suggestive of a near-surface fault. However, detailed models based on gravity and magnetic data were unable to determine whether the anomalies reflect faults or folds (Magsino et al., 2003).

A magnetic contact (Figure 12, label CRF) coincides approximately with the Canyon River fault (Walsh and Logan, 2007) and extends 5 km northeastward beyond its mapped surface expression (Schuster, 2005). High-resolution aeromagnetic data do not cover the western end of the Canyon River fault. The Canyon River fault is expressed topographically as a 3-m-high northwest-facing scarp. A trench excavated across the scarp revealed evidence for oblique reverse-left-lateral slip during a M 7 to 7.5 earthquake in late Holocene time (Walsh and Logan, 2007). The sense of the magnetic contact is consistent with southeast-side-up slip seen in the trench. Although the Canyon River fault is essentially on strike with the Saddle Mountain fault, magnetic anomalies provide no obvious way to connect them as a single, continuous structure. If the Canyon River and Saddle Mountain faults are linked, it is apparently accomplished through complex en echelon relationships.

DISCUSSION

The Saddle Mountain fault is expressed topographically over a length of 15 km, and magnetic anomalies suggest that the fault extends an additional 5 km to the southwest (Figure 12) and 15 km to the northeast (Figure 15), a total span of 35 km. Moreover, the alignment of the Saddle Mountain, Frigid Creek, and Canyon River faults (Figures 11 and 12) may reflect a zone of faulting extending more than 45 km. The opposing sense of slip on these three faults (southeast-side-up reverse slip on the Saddle Mountain and Canyon River faults, northwest-side-up normal slip on the Frigid Creek fault) may reflect their positions relative to deformational patterns in the Puget Lowland immediately to the east (Figure 1): The Saddle Mountain and Canyon River faults are adjacent to the Seattle and Olympia uplifts, respectively, whereas the Frigid Creek fault lies adjacent to the subsiding Dewatto and Tacoma basins. Alternatively, the Frigid Creek fault could

represent either a releasing bend fault or a bending moment normal fault in the hanging wall of the Saddle Mountain fault zone.

Wilson et al. (1979) noted that the Saddle Mountain fault lies on strike with a narrow zone of fracturing mapped by Glassley (1974) immediately to the northeast. Glassley (1974) viewed this fracture zone as a remanent of a major tectonic event that brought lower- and upper-member basalts into contact in Miocene time, and Wilson et al. (1979) suggested that Holocene displacement on the Saddle Mountain fault may reflect a reactivation of this Miocene structure. Recent work by Hirsh and Babcock (2006) has shown, however, that the upper-member–lower-member contact is more likely an abrupt change in metamorphic grade, with lower-member basalt having been altered to greenschist facies. Moreover, Figure 12 shows that the Saddle Mountain fault, as displayed in both lidar and aeromagnetic data, is not coincident with the upper-member-lower-member contact but rather lies 2 to 3 km to the southeast.

Possible structural connection between the Saddle Mountain and Seattle faults

The circular shaped anomaly at the eastern edge of our study area (Figure 11, label GM—Green Mountain) is caused by highly magnetic rocks in the hanging wall of the Seattle and Tacoma faults. The southern margin of anomaly GM lies along the Tacoma fault (Johnson et al., 2004a; Sherrod et al., 2004); the northern margin along the Seattle fault (Blakely et al., 2002). Crescent Formation basalt and Tertiary intrusive rocks exposed at Green and Gold Mountain near the northern edge of anomaly GM probably represent the source of the entire anomaly; likewise the broad limits of anomaly GM predict where these magnetic rocks are located at relatively shallow depth within the Seattle uplift.

Crescent Formation, exposed at the surface in the hanging wall of the Seattle fault, lies 9 to 10 km deep beneath the Seattle basin immediately to the north (Brocher et al., 2001). Widely divergent models have been proposed to explain this large vertical offset: Johnson et al. (1994), Pratt et al. (1997), and ten Brink et al. (2002) envisioned two or three south-dipping thrust faults that extend to depths of 10 to 20 km, bringing the hanging wall of the Seattle fault northward over the Seattle basin. Brocher et al. (2004)

and Kelsey et al. (2008), on the other hand, found evidence for a roof thrust that merges at shallow (<5 km) depth with a south-dipping floor thrust well north of Crescent Formation exposures, thus forming a northward advancing crustal wedge. In their model, large vertical offset in Crescent Formation is accomplished along one or more south-dipping imbricate thrust faults within the wedge (see Fig. 8, Brocher et al., 2004).

Both models require a means to accommodate strain beyond the westward limit of the Seattle fault. Johnson et al. (1994) proposed the existence of a north- to northeast-striking strike-slip fault beneath Hood Canal that transfers strain on the Seattle fault northward to other faults, possibly the southern Whidbey Island fault (Figure 1, dotted line). Although the linear nature of Hood Canal lends credence to this interpretation, no seismic evidence has been found yet to support the existence of a fault beneath and parallel to Hood Canal (Haug, 1998). The magnetic analysis shown in Figure 11 also shows no evidence for a Hood Canal fault, although the altitude of the aeromagnetic survey in this area exceeded 1400 m above ground because of the proximity of the Olympic Mountains range front. A prominent magnetic gradient does lie west and parallel to part of Hood Canal (Figure 11c), but the broad gradient is inconsistent with strike-slip faulting. It more likely reflects the eastward dipping contact between Eocene Crescent Formation of the Olympic Peninsula and younger overlying sediments of the Seattle basin (Figure 8). This contact presumably forms a broad syncline beneath Hood Canal, shallowing eastward within the Seattle uplift, where it produces anomaly GM (Figure 11). As an alternative to faulting along Hood Canal, we identified several prominent magnetic anomalies in the northern part of our study area (Figure 11c, label DBF—Dabob Bay fault) with abrupt, linear, northwest-striking gradients. They may reflect right-lateral strike-slip faults that pass through Dabob Bay and transfer strain from the Seattle fault northward.

We propose that the Saddle Mountain fault forms part of the western boundary of the Seattle uplift. As evidence, we note a subtle west-striking magnetic lineament (Figure 15, label SF) that lies on strike with the Seattle fault to the east, crosses Hood Canal, and extends westward 10 km into Crescent Formation volcanic rocks to the west. At its western end, within Crescent Formation exposures, anomaly SF passes through a pronounced 3- to 4-km right-step in magnetic anomalies and mapped folds (Tabor and

Cady, 1978b). The westward terminus of lineament SF lies near the northern terminus of the Saddle Mountain fault (Figure 15, label SMF). We suggest that lineament SF is the westward extension of the Seattle fault.

We suggest that the Saddle Mountain, Frigid Creek, and Canyon River faults are elements of a deformation zone that accommodate the northward shortening of Puget Lowland crust inboard of the Olympic massif (label SMDZ—Saddle Mountain deformation zone, Figure 16). This model predicts sinistral slip on all elements of the Saddle Mountain deformation zone. We also expect vertical slip to be important, with sense determined by the proximity of large-scale deformation to the east: The Saddle Mountain and Canyon River faults (southeast-side-up) respond to the Seattle and Olympia uplifts, respectively, whereas the Frigid Creek fault (northwest-side-up) is influenced by subsidence of the Dewatto and Tacoma basins. Lineament SF (Figure 15) may be the westward continuation of the Seattle fault, with the Saddle Mountain fault (Figure 15, label SMF) marking the western edge of the Seattle uplift.

CONCLUSIONS

We propose that the Saddle Mountain, Frigid Creek, and Canyon River faults are elements of a 45 km-long zone of deformation that accommodates shortening of Puget Lowland crust inboard of the Olympic massif. We see subtle evidence in geophysical anomalies that the Seattle fault extends westward across Hood Canal and 10 km into Crescent Formation exposures on the Olympic Peninsula, ending near the northern terminus of the Saddle Mountain deformation zone. In this framework, the Saddle Mountain and Seattle faults are boundaries of the same crustal block, the Seattle uplift. Previous studies have shown that the Saddle Mountain fault produced a M_W 6.5 to 7.0 earthquake 1000-1300 ka, within the same century as the M_W 7.5 Seattle fault earthquake. The temporal coincidence of these two earthquakes suggests that the Saddle Mountain deformation zone and Seattle fault zone are kinematically linked, and our geophysical studies further suggest that the two fault zones are spatially linked as well. We have mapped a magnetic contact that coincides with the topographic expression of the Saddle Mountain fault and shows that it extends at least 35 km. A magnetic survey of

Price Lake conducted from a nonmagnetic canoe has allowed us to model the Saddle Mountain West fault in detail. The model includes two east-dipping reverse faults, consistent with scarps identified in lidar data and in the field. The opposing sense of slip on the Saddle Mountain, Frigid Creek, and Canyon River faults (southeast-side-up reverse slip on the Saddle Mountain and Canyon River faults, southeast-side-down normal slip on the Frigid Creek fault) may be a reflection of deformational patterns in the Puget Lowland immediately to the east. The Saddle Mountain and Canyon River faults lie adjacent to the Seattle and Olympia uplifts, whereas the Frigid Creek fault lies near the subsiding Dewatto and Tacoma basins.

ACKNOWLEDGMENTS

We are grateful to Jerry Kvale, Washington Department of Natural Resources, for providing access to Price Lake. Tom Wiley graciously provided unpublished gravity data from the southeast Olympic Mountains. We also thank Tom Brocher, Gerry Connard, Jonathan Glen, Darcy McPhee, Rowland Tabor, and Rob Witter for helpful discussions and critical readings of early versions of our manuscript. Very helpful reviews were provided by Harvey Kelsey and Cathy Snelson.

REFERENCES CITED

Atwater, B.F., and Moore, A.L., 1992, A tsunami ~1000 yr ago in Puget Sound, Washington: Science, v. 258, p. 1614-1617.

Babcock, R.S., Burmester, R.F., Engebretson, D.C., Warnock, A., and Clark, K.P., 1992, A rifted margin origin for the Crescent basalts and related rocks in the northern Coast Range volcanic province, Washington and British Columbia: Journal of Geophysical Research, v. 97, p. 6799-6821.

Blakely, R.J., Wells, R.E., and Weaver, C.S., 1999, Puget Sound aeromagnetic maps and data: U.S. Geological Survey Open-File Report 99–514, http://geopubs.wr.usgs.gov/open-file/of99-514.

Blakely, R.J., Wells, R.E., Weaver, C.S., and Johnson, S.Y., 2002, Location, structure, and seismicity of the Seattle fault zone, Washington: Bulletin of the Geological Society of America, v. 114, p. 169-177.

Brandon, M.T., Roden-Tice, M.K., and Garver, J.I., 1998, Late Cenozoic exhumation of the Cascadia accretionary wedge in the Olympic Mountains, northwest Washington State: Geological Society of America Bulletin, v. 110, p. 985-1009.

Brocher, T.M., Blakely, R.J., and Wells, R.E., 2004, Reinterpretation of the Seattle uplift, Washington, as a passive roof duplex: Bulletin of the Seismological Society of America, v. 94, p. 1379-1401.

Brocher, T.M., Parsons, R.J., Blakely, R.J., Christensen, N.I., Fisher, M.A., Wells, R.E., and the SHIPS Working Group, 2001, Upper crustal structure in Puget Lowland, Washington: Results from the 1998 Seismic Hazards Investigation in Puget Sound: Journal of Geophysical Research, v. 106, p. 13,541–13,564.

Brown, R.D., Jr., Gower, H.D., and Snavely, P.D., Jr., 1960, Geology of the Port Angeles—Lake Crescent area, Clallam County, Washington: U.S. Geological Survey Oil and Gas Investigations Map OM-203, scale 1:62,500.

Bucknam, R.C., Hemphill-Haley, E., and Leopold, E.B., 1992, Abrupt uplift within the past 1700 years at southern Puget Sound, Washington: Science, v. 258, p. 1611-1614.

Cady, W.M., 1975, Tectonic setting of the Tertiary volcanic rocks of the Olympic Peninsula, Washington: U.S. Geological Survey Journal of Research, v. 3, p. 573-582.

Carson, R.J., 1973, First known active fault in Washington: Washington Geologic Newsletter, Washington Division of Geology and Earth Resources, v. 1, no. 3, p. 1-2.

Carson, R.J., and Wilson, J.R., 1974, Quaternary faulting on Dow Mountain, Mason County: Washington Division of Geology and Earth Resources Open-File Report 76-2, scale 1:62,500.

Glassley, W., 1974, Geochemistry and tectonics of the Crescent volcanic rocks, Olympic Peninsula, Washington: Geological Society of America Bulletin, v. 85, p. 785-794.

Haug, B. J., 1998, High-resolution seismic reflection interpretations of the Hood Canal-Discovery Bay fault zone; Puget Sound, Washingtion: M.S. Thesis, Portland State University, http://nwdata.geol.pdx.edu/Thesis/FullText/1998/Haug/

Haugerud, R.A., Harding, D.J., Johnson, S.Y., Harless, J.L., Weaver, C.S., and Sherrod, B.L., 2003, High-resolution lidar topography of the Puget Lowland, Washington—A bonanza for earth science: GSA Today, v. 13, no., 6, p. 4-10.

Haugerud, R.A., and Sherrod, B.L., 2007, Geomorphic evidence for Holocene tectonism in western Washington [abstract]: 103rd Annual Meeting of the Cordilleran Section, Geological Society of America, Bellingham, Washington, May 2007, Paper 22-3.

Hirsch, D.M., and Babcock, S., 2006, Unexpected vertical variations in metamorphism within the Crescent basalt, Dosewallips River valley, Olympic Peninsula, Washington: Geological Society of America Abstracts with Programs, v. 38, no. 5, p. 18.

Hughes, J.F., 2005, Meters of synchronous Holocene slip on two strands of a fault in the western Puget Sound lowland, Washington [abstract]: EOS Transactions AGU, v. 86, no 52, Fall Meeting Supplement, Abstract S51C-1020.

Johnson, S.Y., Blakely, R.J., Stephenson, W.J., Dadisman, S.V., and Fisher, M.A., 2004a, Active shortening of the Cascadia forearc and implications for seismic hazards of the Puget Lowland: Tectonics. V. 23. TC1011, doi:10.1029/2003TC001507.

Johnson, S.Y., Nelson, A.R., Personius, S.F., Wells, R.E., Kelsey, H.M., Sherrod, B.L., Okumura, K., Koehler III, R., Witter, R.C., Bradley, L., and Harding, D.J., 2004b, Evidence for late Holocene earthquakes on the Utsalady Point fault, northern Puget Lowland, Washington: Bulletin of the Seismological Society of America, v. 94, p. 2299-2316.

Johnson, S.Y., Potter, C.J., and Armentrout, J.M., 1994, Origin and evolution of the Seattle fault and Seattle basin, Washington: Geology, v. 22, p. 71-74.

Johnson, S.Y., Potter, C.J., Armentrout, J.M., Miller, J.J., Finn, C.A., and Weaver, C.S., 1996, The southern Whidbey Island fault, an active structure in the Puget Lowland, Washington: Geological Society of America Bulletin, v. 108, p. 334-354.

Karlin, R., and Abella, S.E., 1996, A history of Pacific Northwest earthquakes recorded in Holocene sediments from Lake Washington: Journal of Geophysical Research, v. 1030, p. 6137-6150.

Kelsey, H.M., Sherrod, B.L., Johnson, S.Y., and Dadisman, S.V., 2004, Land-level changes from a late Holocene earthquake in the northern Puget Lowland, Washington: Geology, v. 32, p. 469-472.

Kelsey, H.M., Sherrod, B.L., Nelson, A.R., and Brocher, T.M., 2008, Earthquakes generated from bedding-plane-parallel reverse faults above an active wedge thrust: Geological Society of America Bulletin, v. 120, in press.

Logan, R.L., Schuster, R.L., Pringle, P.T., Walsh, T.J., and Palmer, S.P., 1998, Radiocarbon ages of probable coseismic features from the Olympic Peninsula and Lake Sammamish, Washington: Washington Geology, v. 26, p. 59-67.

Magsino, S., Sanger, E., Walsh, T.J., Palmer, S.P., and Blakely, R.J., 2003, The Olympia structure; ramp or discontinuity? New gravity data provide information: Abstracts with Programs, Geological Society of America, v. 35, n. 6, p. 479.

Marshall, M., and Cox, A., 1972, Magnetic changes in pillow basalt due to sea floor weathering: Journal of Geophysical Research, v. 77, p. 6459-6469.

Mazzotti, S., Dragert, H., Hyndman, R.D., Miller, M.M., and Henton, J.A., 2002, GPS deformation in a region of high crustal seismicity—N. Cascadia forearc: Earth and Planetary Science Letters, v. 198, p. 41-48.

McCaffrey, R., Qamar, A., King, R.W., Wells, R.E., Khazaradze, G., Williams, C.A., Stevens, C.W., Vollick, J.J., and Zwick, P.C., 2007, Fault locking, block rotation and crustal deformation in the Pacific Northwest: Geophysical Journal International, doi: 10.1111/j.1365-246X.2007.03371.x.

Nelson, A.R., Johnson, S.Y., Kelsey, H.M., Wells, R.E., Sherrod, B.L., Pezzopane, S.K., Bradley, A., Koehler III, R.D., and Bucknam, R.C., 2003, Late Holocene earthquakes on the Toe Jam Hill fault, Seattle fault zone, Bainbridge Island, Washington: Geological Society of America, v. 115, p. 1388-1403.

Nelson, A.R., Personius, S.F., Buck, Jason, Bradley, L.-A., Wells, R.E., and Schermer, E.R., 2007, Field and laboratory data from an earthquake history study of scarps of the Lake Creek–Boundary Creek fault between the Elwha River and Siebert

Creek, Clallam County, Washington: U.S. Geological Survey Scientific Investigations Map 2961, 2 sheets.

Phillips, J.D., Hansen, R.O., and Blakely, R.J., 2007, The use of curvature in potential-field interpretation: Exploration Geophysics, v. 28, p. 111-119.

Pratt, T.L., Johnson, S. Potter, C., Stephenson, W., and Finn, C., 1997, Seismic reflection images beneath Puget Sound, western Washington State: the Puget lowland thrust sheet hypothesis, Journal of Geophysical Research, v. 102, p. 27469-27489.

Schuster, J.E., 2005, Geologic map of Washington State: Washington Division of Geology and Earth Resources, Geologic Map GM-53, scale 1:250,000.

Schuster, R.L., Logan, R.L., and Pringle, P.T., 1992, Prehistoric rock avalanches in the Olympic Mountains, Washington: Science, v. 258, p. 1620-1621.

Sherrod, B.L., 2001, Evidence for earthquake-induced subsidence ~1100 yr ago in coastal marshes of southern Puget Sound, Washington: Geological Society of America Bulletin, v. 113, p. 1299-1311.

Sherrod, B.L., Blakely, R.J., Weaver, C.S., Kelsey, H.M., Barnett, E., Liberty, L., Meagher, K.L., and Pape, K., 2008, Finding concealed active faults: Extending the southern Whidbey Island fault across the Puget Lowland, Washington: Journal of Geophysical Research, v. 113, B05313, doi:10.1029/2007/JB005060.

Sherrod, B.L., Brocher, T.M., Weaver, C.S., Bucknam, R.C., Blakely, R.J., Kelsey, H.M., Nelson, A.R., and Haugerud, R., 2004, Holocene fault scarps near Tacoma, Washington, USA: Geology, v. 32, p. 9-12.

Simpson, R.W., Jachens, R.C., Blakely, R.J., and Saltus, R.W., 1986, A new isostatic residual gravity map of the conterminous United States with a discussion of the significance of isostatic residual anomalies: Journal of Geophysical Research, v. 91, p. 8348-8372.

Snavely, P.D., Jr., and Wagner, H.C., 1963, Tertiary geologic history of western Oregon and Washington: Washington Division of Mines and Geology Report of Investigation 22, 25 p.

Tabor, R.W., and Cady, W.M., 1978a, The structure of the Olympic Mountains, Washington—analysis of a subduction zone: U.S. Geological Survey Professional Paper 1033, 25 p.

Tabor, R.W., and Cady, W.M., 1978b, Geologic map of the Olympic Peninsula, Washington: U.S. Geological Survey Miscellaneous Investigations Series Map I-994, scale 1:125,000.

ten Brink, U.S., Molzer, P.C., Fisher, M.A., Blakely, R.J., Bucknam, R.C., Parsons, T., Crosson, R.S., and Creager, K.C., 2002, Subsurface geometry and evolution of the Seattle fault zone and the Seattle basin: Bulletin of the Seismological Society of America, v. 92, p. 1737-1753.

ten Brink, U.S., Song, J., and Bucknam, R.C., 2006, Rupture models for the A.D. 900-930 Seattle fault earthquake from uplifted shorelines: Geology, v. 34, p. 585-588, doi: 10.1130/G22173.1.

Walsh, T.J., and Logan, R.L., 2007, Field data for a trench on the Canyon River fault, southeast Olympic Mountains, Washington: Washington Division of Geology and Earth Resources, Open-File Report 2007-1.

Washington Division of Geology and Earth Resources Staff, 2005, Digital 1:100,000-scale Geology of Washington State, Version 1.0: Washington State Department of Natural Resources, Division of Geology and Earth Resources, Open File Report 2005-3.

Wells, R.E., Weaver, C.S., and Blakely, R.J., 1998, Fore-arc migration in Cascadia and its neotectonic significance: Geology, v. 26, p. 759-762.

Wilson, J.R., 1975, Geology of the Price Lake area, Mason County, Washington: Raleigh, North Carolina State University, M.S. thesis, 99 p.

Wilson, J.R., Bartholomew, M.J., and Carson, R.J., 1979, Late Quaternary faults and their relationship to tectonism in the Olympic Peninsula, Washington: Geology, v. 7, p. 235-239.

Witter, R.C., and Givler, R.W., 2008, Two post-glacial earthquakes on the Saddle Mountain West fault, southeastern Olympic Peninsula, Washington: Bulletin of the Seismological Society of America, in press.

Table 1. Magnetic susceptibilities measured in situ at various site localities in the eastern and southeastern Olympic Peninsula. ID is site identification. LON and LAT are longitude west and latitude north, respectively, of sample site, datum NAD83. AVG and SD are geometric average and standard deviation of N samples expressed. Magnetic susceptibility is a dimensionless physical property of the rock here expreseed in SI units (Systèms Internationale) multiplied by 1000. Samples typically span a distance of several tens of meters at each site.

ID	LON	LAT	AVG	SD	N
S1	123.12087	47.43788	3.508	1.883	12
S2	123.04327	47.53535	31.750	4.669	12
S3	123.00597	47.58107	19.077	6.152	13
S4	122.96822	47.61942	23.041	9.787	13
S5	122.93480	47.79580	15.463	8.822	18
S6	122.96897	47.78395	17.211	12.236	18
S7	122.98283	47.78728	25.877	9.147	13
S8	122.99423	47.78737	13.225	4.769	13
S9	123.00480	47.79002	9.643	5.397	16
S10	123.01965	47.78895	34.967	17.217	13
S11	123.02770	47.79092	21.236	6.276	13
S12	123.03822	47.79037	7.566	7.422	13
S13	123.04347	47.78387	18.422	10.181	13
S14	123.05188	47.78162	48.192	19.298	13
S15	122.90770	47.81445	37.693	17.857	13
S16	122.91375	47.80822	12.440	7.581	13
S17	122.91908	47.77365	24.833	10.749	12
S18	122.99112	47.72142	14.377	3.543	13
S19	123.02725	47.73852	7.801	11.700	13

S20	123.00945	47.72530	32.362	10.559	13
S21	123.25702	47.49587	8.398	5.105	13
S22	123.27960	47.49467	10.084	6.707	13
S23	123.30593	47.49840	4.225	3.648	13
S24	123.32262	47.50957	15.778	18.805	13
S25	123.14502	47.46843	19.350	4.544	12
S26	123.14157	47.46773	33.238	10.988	13
S27	123.15457	47.45260	23.569	11.435	12
S28	123.16308	47.46155	31.078	28.094	13
S29	123.15372	47.48100	21.888	13.428	13
S30	123.17503	47.47798	31.951	9.967	13
S31	123.04422	47.56798	26.926	10.676	12
S32	123.07630	47.58083	29.462	13.834	13
S33	123.10688	47.58770	14.845	13.910	13
S34	123.12152	47.60060	2.717	2.442	13
S35	123.12327	47.61157	8.725	7.606	13
S36	123.10755	47.62243	10.173	6.575	13
S37	123.16868	47.59852	0.582	0.094	13
S38	123.18233	47.59468	16.982	10.523	13
S39	123.18907	47.59222	0.652	0.122	12
S40	123.20110	47.58562	3.066	3.097	13
S41	123.22337	47.58227	9.688	7.665	13
S42	123.25307	47.57943	0.168	0.038	13
S43	123.26108	47.57527	0.205	0.045	14
S44	123.25083	47.58017	0.174	0.064	13
S45	123.08065	47.57123	18.265	8.815	13
S46	123.07438	47.55302	7.599	1.659	10

S47	123.06255	47.52713	21.000	6.752	13

FIGURE CAPTIONS

Figure 1. (A) Topographic map of northwestern Washington and Vancouver Island. Bold lines are faults modified from Washington Division of Geology and Earth Resources (2005). B, Bellingham; E, Everett; S, Seattle; T, Tacoma; O, Olympia; V, Victoria. (B) Isostatic residual gravity anomalies. BB, Bellingham basin; EB, Everett basin; SB, Seattle basin; TB, Tacoma basin; DB, Dewatto basin; DMF, Devils Mountain fault; SPF, Strawberry Point fault; UPF, Utsulady Point fault; SF, Seattle fault; TF, Tacoma fault; SWIF, southern Whidbey Island fault; SMF, Saddle Mountain fault; FCF, Frigid Creek fault; CRF, Canyon River fault; OF, Olympia fault. Dotted line is Hood Canal fault. Blue rectangles indicate areas of Figures 2, 4, and 6.

Figure 2. Lidar image of the area between Lake Cushman and Hood Canal. See Figure 1 for map location. Both maps A and B show same lidar image; map B includes labels and lines to identify scarps and other physiographic features discussed in text. Red lines are scarps identified from lidar images. White circles are locations of older trench excavations (Wilson, 1975; Wilson et al., 1979). Orange circle is location of more recent trench excavation described by Witter and Givler (2008). Dashed rectangles show areas of Figures 3, 9, and 13.

Figure 3. Lidar image of Price Lake area. See Figure 2 for location. Both maps A and B show same lidar image. Red lines on map B indicate scarps identified from lidar image. Insets A, B, C, and D are topographic profiles across the Saddle Mountain East strand.

Figure 4. Geologic map of the study area, modified from Schuster (2005). See Figure 1 for map location. White dotted line is mapped contact between upper- and lower-member Crescent Formation (Tabor and Cady, 1978b). Red dashed line indicates location of geologic cross section shown in Figure 8. Black dashed rectangles show locations of maps in Figures 12 and 15. Black lines are faults, dotted where concealed. SMF, Saddle Mountain fault; FCF, Frigid Creek fault; CRF, Canyon River fault; LM and UM, lower and upper members of the Crescent Formation, respectively.

Figure 5. Model for the Olympic Peninsula accretionary complex, modified from Tabor and Cady (1978a).

Figure 6. (A) Aeromagnetic anomalies (Blakely et al., 1999) of the study area. See Figure 1 for map location. Colored circles indicate location and magnitude of magnetic susceptibility measurements (Table 1). (B) Isostatic residual gravity anomalies. White solid lines with barbs are thrust faults from Figure 4; white solid lines without barbs outline Crescent Formation exposures. White dotted line is geologically mapped contact between lower- and upper-member Crescent Formation (Tabor and Cady, 1978b). Red dashed line indicates location of geologic cross section shown in Figure 8.

Figure 7. Graph showing magnetic susceptibility measurements (Table 1) as a function of magnetic anomaly amplitude at the same locations. Error bars are ±1 standard deviation. Sites are from the area near Lake Cushman and Price Lake and thus are a subset of the sites shown on Figure 6a.

Figure 8. Geologic cross section derived by forward modeling of magnetic and gravity data. (A) Calculated and observed magnetic anomaly. (B) Calculated and observed gravity anomaly. (C) Magnetic distribution derived by simultaneous modeling of gravity and magnetic profiles. Model assumed to extend to infinity in both directions perpendicular to profile. (D) Geologic interpretation of magnetic model. Figures 4 and 6 show location of profile. $\Delta\rho$, density contrast relative to normal crust (2670) in kg/m^3; χ, magnetic susceptibility in SI units multiplied by 1000.

Figure 9. Magnetic anomalies over Price Lake, measured with nonmagnetic canoe. See Figure 2 for map location. Base map is lidar image of Figure 2. Black dotted lines show location of canoe transects. Tick marks are UTM coordinates in meters. White dashed lines indicate magnetic trough on strike with lidar scarps (red lines). Dashed yellow line shows location of cross section shown in Figure 10.

Figure 10. Cross-sectional interpretation of Saddle Mountain West fault using canoe-based magnetic-survey data. χ, assumed magnetic susceptibility in SI (Systèms

Internationale) units. Model assumed to extend to great distances in the direction perpendicular to the profile direction. Dotted lines are faults inferred from modeled unit offsets. See Figure 9 for location of profile.

Figure 11. Regional interpretation of the eastern and southeastern Olympic Peninsula, based on gravity and magnetic anomalies. (A) Geologic map, modified from Schuster (2005). White dotted line is contact between upper- and lower-member Crescent Formation (Tabor and Cady, 1978b). (B) Aeromagnetic anomalies. Black dots indicate abrupt magnetization variations, calculated directly from aeromagnetic anomalies shown in background. Dots on this map often coalesce together and form the appearance of continuous lines. (C) Interpretation of geophysical data. CPF, thrust contact between core sedimentary rocks and peripheral volcanic rocks; DBF, possible en echelon faults through Dabob Bay; SF, possible westward extension of the Seattle fault; TF, Tacoma fault; OF, Olympia fault; SMF, Saddle Mountain fault; FCF, Frigid Creek fault; CRF, Canyon River fault; GM, Green and Gold Mountain.

Figure 12. Interpretation of aeromagnetic anomalies and lidar scarps in the Saddle Mountain area. See Figure 4 for map location. (A) Aeromagnetic anomalies shown as rainbow colors. Black lines indicate lidar scarps. Color dots are abrupt variations in magnetization calculated directly from magnetic anomalies. Dots are colored according to relative significance, with warm colors more significant than cool colors. Along magnetic gradients, individual dots are very close together and appear as solid lines. (B) Interpretation. See caption to Figure 11 for label definitions.

Figure 13. Lidar image of Frigid Creek area. See Figure 2 for map location. Both maps A and B show same lidar image. Red lines on map B indicate scarps identified from lidar image. White circle is location of Frigid Creek trench (Figure 14).

Figure 14: (A) Log of excavation across the Frigid Creek fault scarp. Small blue dots show locations of radiocarbon ages. (B) Retrodeformation of excavation log. The analysis indicated that 93 percent of the scarp uplift was caused by a single

event in which Block 2 dropped 2.5 m and rotated clockwise 12°, forming a graben, and Block 3 dropped 1.9 m.

Figure 15. Interpretation of aeromagnetic anomalies at the western end of the Seattle fault. See Figure 4 for map location. (A) Aeromagnetic anomalies shown as rainbow colors. Black lines indicate lidar scarps. Color dots are abrupt variations in magnetization, indicative of magnetic contacts. Dots are colored according to relative significance, with warm colors more significant than cool colors. Along magnetic gradients, individual dots are very close to one another and appear as solid lines. (B) Interpretation. Gray arrows indicate north-south horizontal compression. See Figure 11 for label definitions.

Figure 16. Tectonic setting of the Saddle Mountain fault. Red and blue stipple indicates Puget Sound uplift and sedimentary basins, respectively, as defined by regional gravity anomalies. Red lines are faults of the Saddle Mountain deformation zone. Yellow arrows indicate regional strain direction: north-directed compression in the Puget Lowland and northeast-directed compression (parallel to the plate convergence vector) in the Olympic Peninsula. LRF, Leech River fault; RMF, Rattlesnake Mountain fault; WRF, White River fault; SCF, Straight Creek fault; OF, Olympia fault; OU, Olympia uplift; SU, Seattle uplift; KA, Kingston arch. Other labels explained in Figure 1 caption.

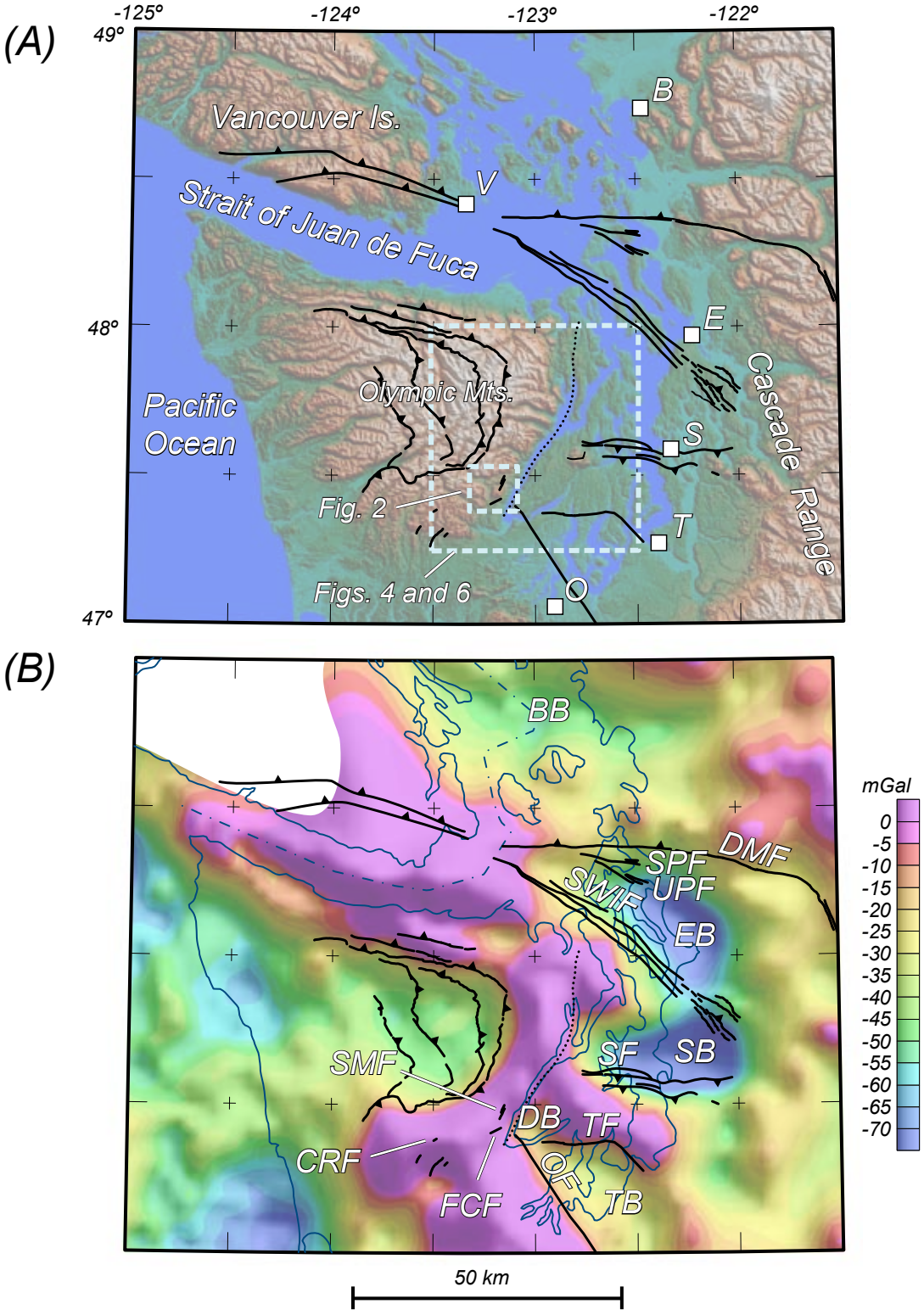
(A)
-125°
-124°
-123°
-122°
49°
48°
47°
Vancouver Is.
Strait of Juan de Fuca
Pacific Ocean
Olympic Mts.
Cascade Range
B
V
E
S
T
O
Fig. 2
Figs. 4 and 6
(B)
BB
DMF
SPF
SWIF
UPF
EB
SF
SB
SMF
DB
TF
CRF
FCF
OF
TB
mGal
0
-5
-10
-15
-20
-25
-30
-35
-40
-45
-50
-55
-60
-65
-70
50 km

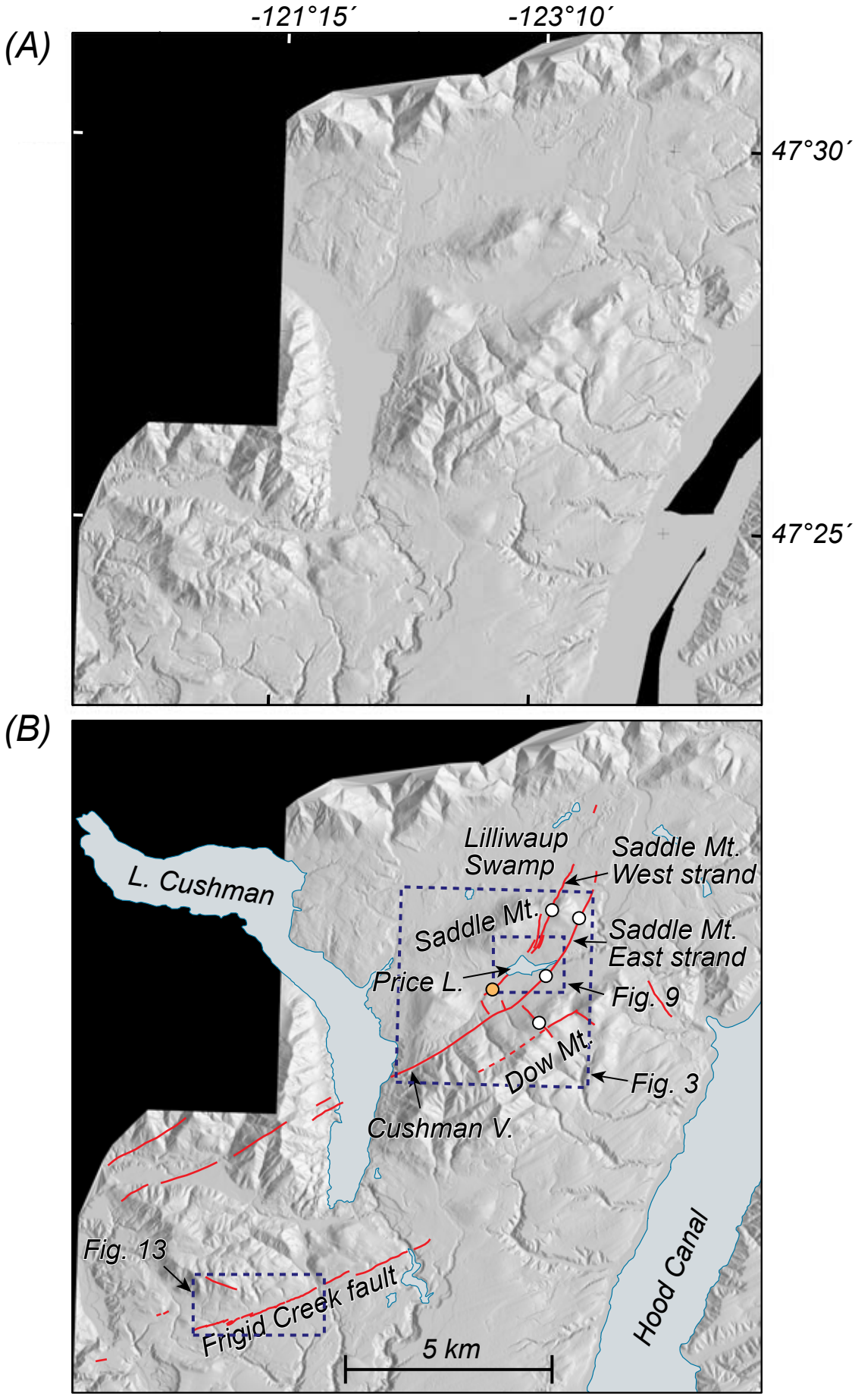
(A)
-121°15´
-123°10´
47°30´
47°25´
(B)
L. Cushman
Lilliwaup Swamp
Saddle Mt. West strand
Saddle Mt.
Saddle Mt. East strand
Price L.
Fig. 9
Dow Mt.
Fig. 3
Cushman V.
Fig. 13
Frigid Creek fault
Hood Canal
5 km

Figure 3

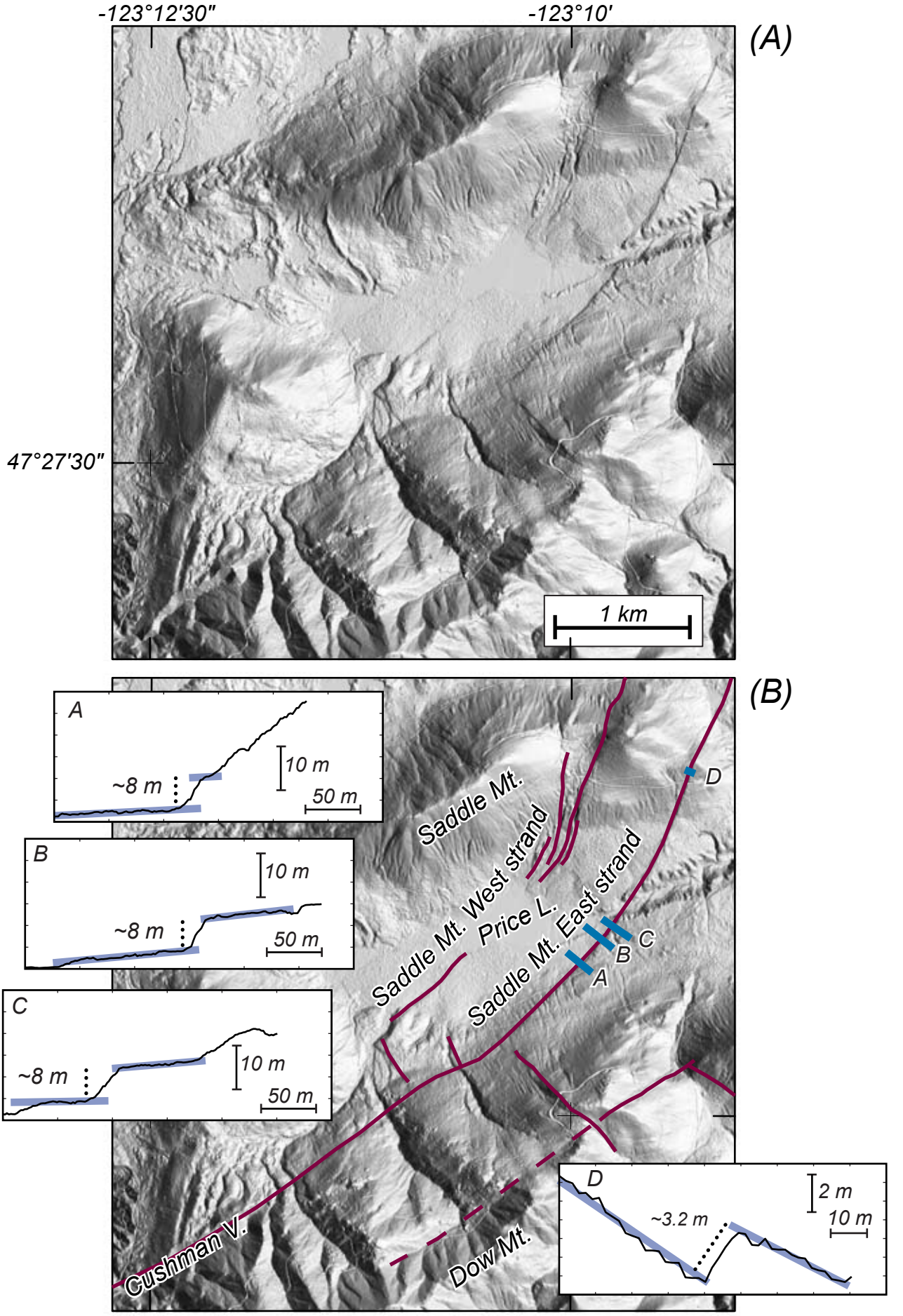
-123°12'30"
-123°10'
47°27'30"
(A)
1 km
(B)
A
~8 m
10 m
50 m
B
~8 m
10 m
50 m
C
~8 m
10 m
50 m
Saddle Mt.
Saddle Mt. West strand
Price L.
Saddle Mt. East strand
A
B
C
D
Cushman V.
Dow Mt.
D
~3.2 m
2 m
10 m

Figure 4

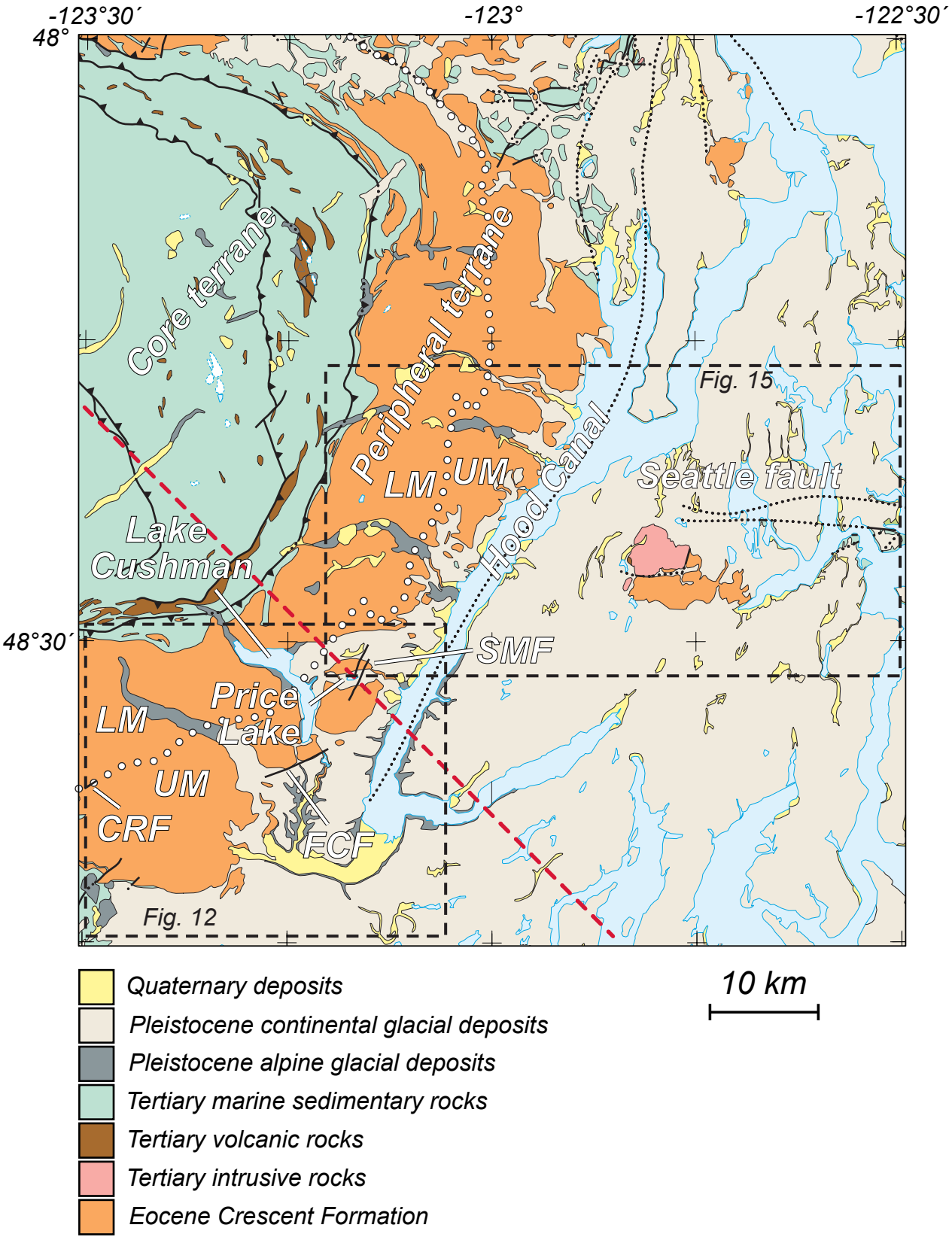
-123°30´
-123°
-122°30´
48°
48°30´
Core terrane
Peripheral terrane
Fig. 15
LM
UM
Hood Canal
Seattle fault
Lake Cushman
SMF
Price Lake
LM
UM
CRF
FCF
Fig. 12
Quaternary deposits
Pleistocene continental glacial deposits
Pleistocene alpine glacial deposits
Tertiary marine sedimentary rocks
Tertiary volcanic rocks
Tertiary intrusive rocks
Eocene Crescent Formation
10 km

Figure 5

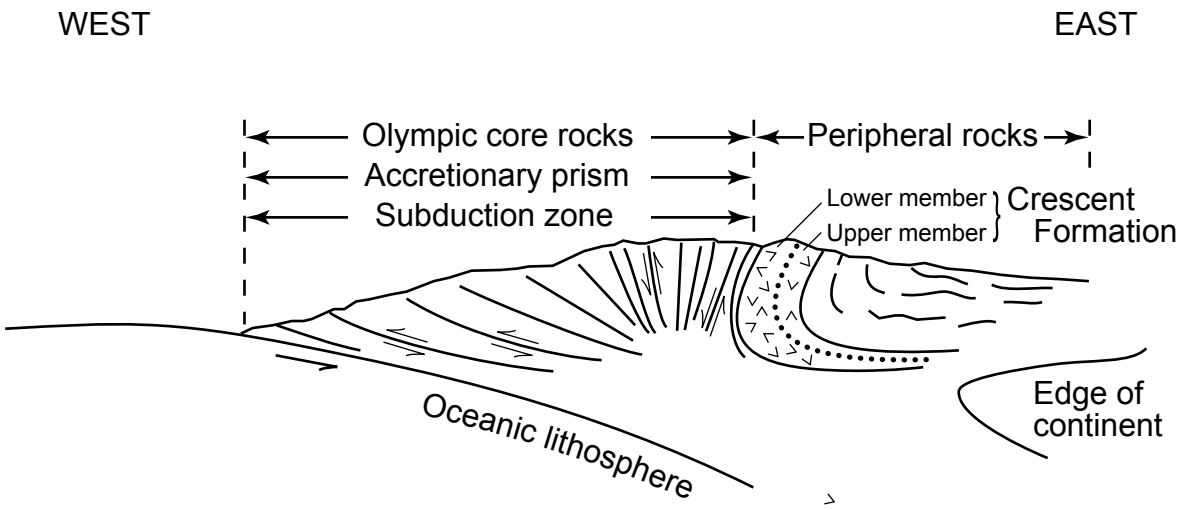
WEST
EAST
Olympic core rocks
Accretionary prism
Subduction zone
Peripheral rocks
Lower member
Upper member
Crescent
Formation
Edge of
continent
Oceanic lithosphere

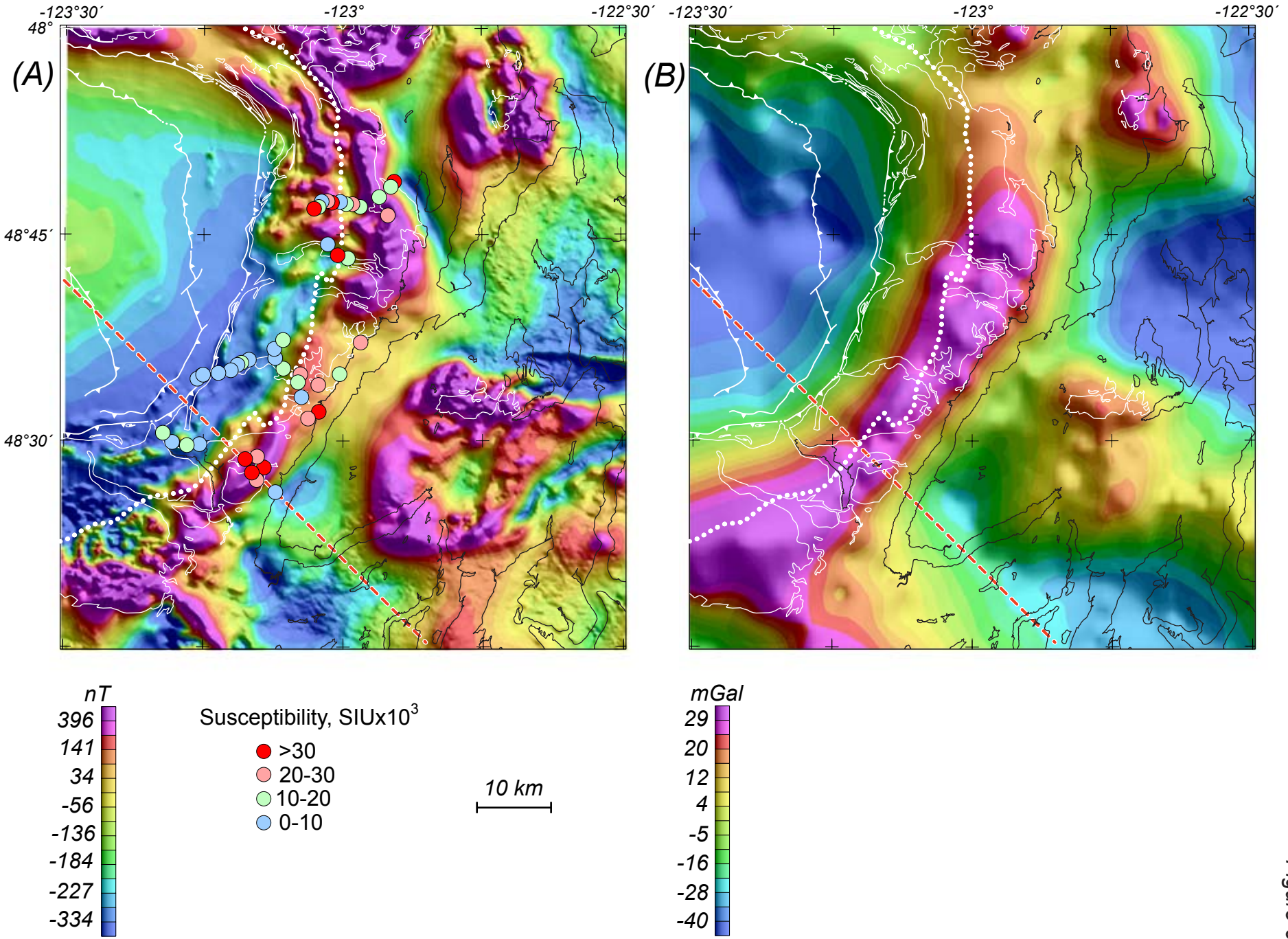
-123°30´
-123°
-122°30´
48°
48°45´
48°30´
(A)
(B)
nT
396
141
34
-56
-136
-184
-227
-334
Susceptibility, SIUx10^3
>30
20-30
10-20
0-10
10 km
mGal
29
20
12
4
-5
-16
-28
-40

Figure 6

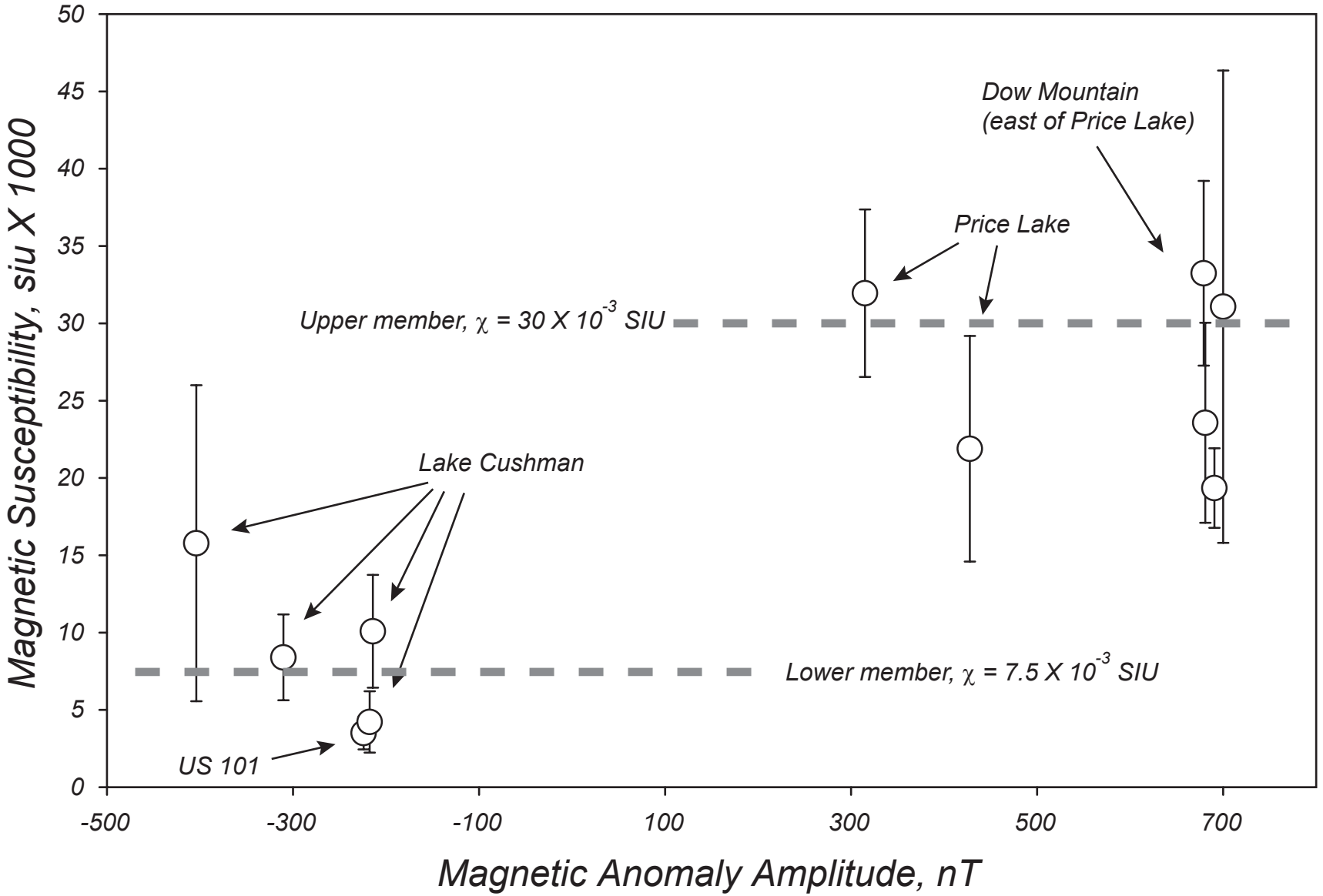
Magnetic Susceptibility, siu X 1000
50
45
40
35
30
25
20
15
10
5
0
-500
-300
-100
100
300
500
700
Magnetic Anomaly Amplitude, nT
Dow Mountain
(east of Price Lake)
Price Lake
Upper member, χ = 30 X 10-3 SIU
Lake Cushman
Lower member, χ = 7.5 X 10-3 SIU
US 101

Figure 7

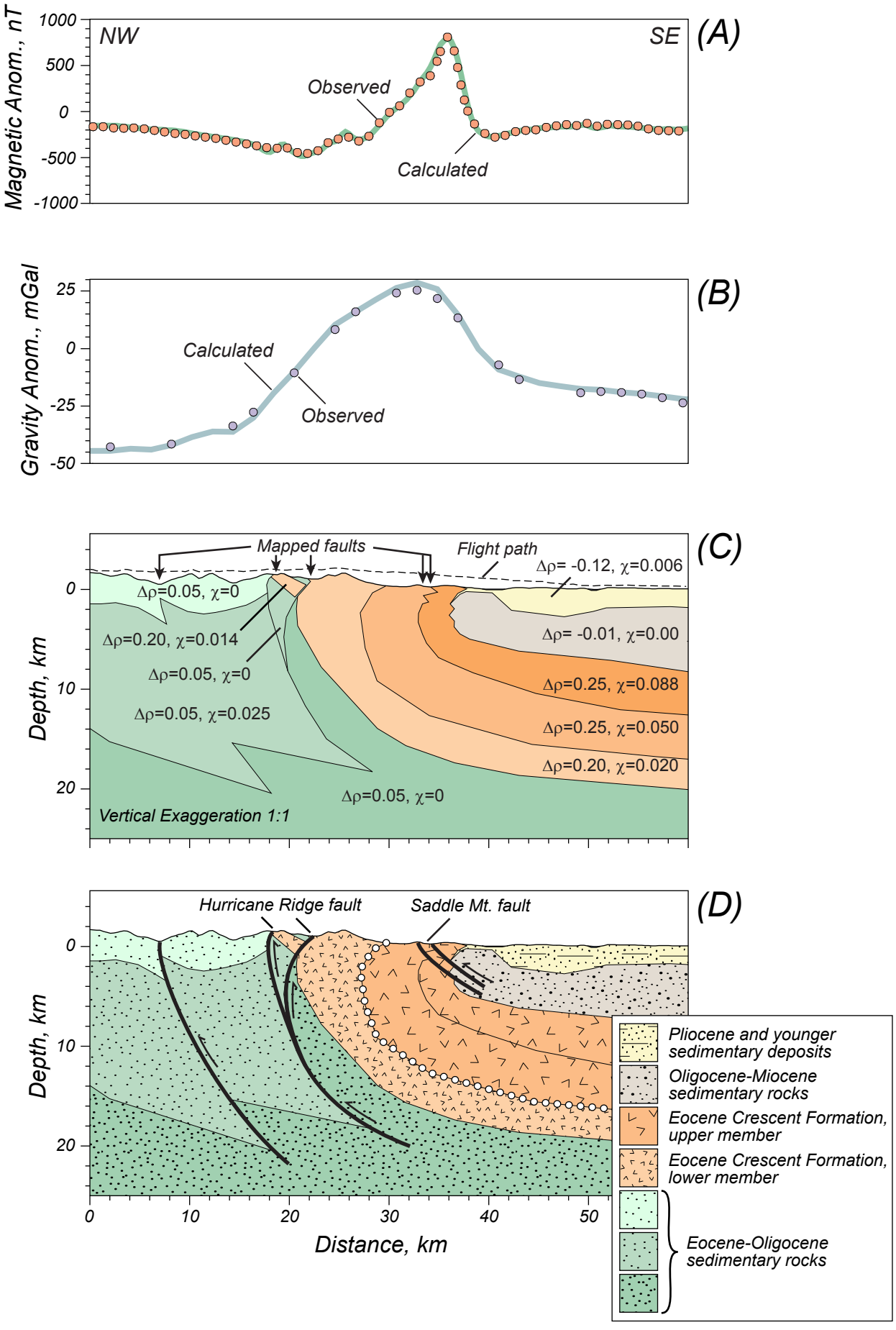
(A)
Magnetic Anom., nT
1000
500
0
-500
-1000
NW
SE
Observed
Calculated
(B)
Gravity Anom., mGal
25
0
-25
-50
Calculated
Observed
(C)
Depth, km
0
10
20
Mapped faults
Flight path
Δρ= -0.12, χ=0.006
Δρ=0.05, χ=0
Δρ=0.20, χ=0.014
Δρ=0.05, χ=0
Δρ=0.05, χ=0.025
Δρ= -0.01, χ=0.00
Δρ=0.25, χ=0.088
Δρ=0.25, χ=0.050
Δρ=0.20, χ=0.020
Δρ=0.05, χ=0
Vertical Exaggeration 1:1
(D)
Depth, km
0
10
20
Hurricane Ridge fault
Saddle Mt. fault
0
10
20
30
40
50
Distance, km
Pliocene and younger sedimentary deposits
Oligocene-Miocene sedimentary rocks
Eocene Crescent Formation, upper member
Eocene Crescent Formation, lower member
Eocene-Oligocene sedimentary rocks

Figure 9

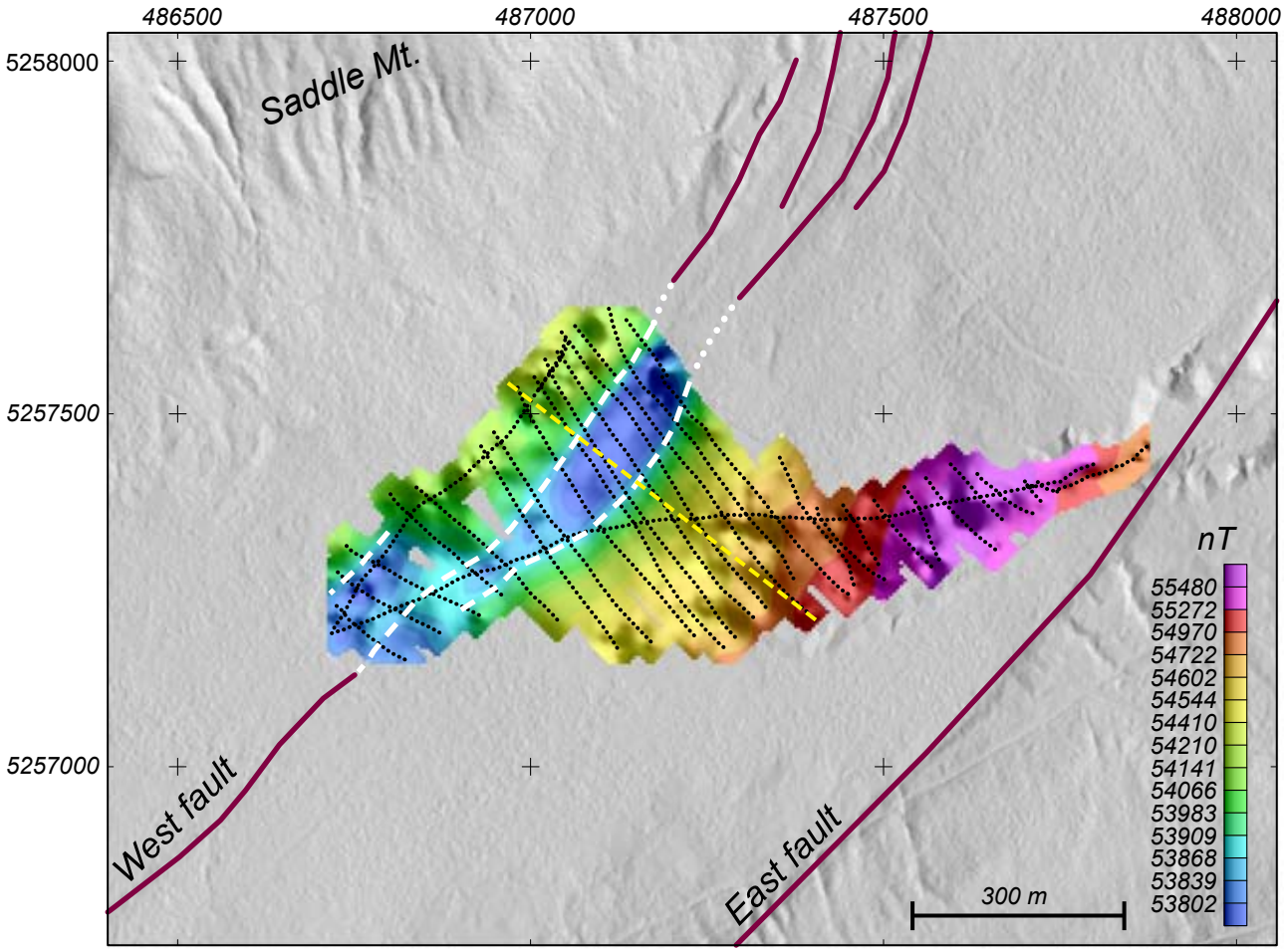
486500
487000
487500
488000
5258000
5257500
5257000
Saddle Mt.
West fault
East fault
300 m
nT
55480
55272
54970
54722
54602
54544
54410
54210
54141
54066
53983
53909
53868
53839
53802

Figure 10

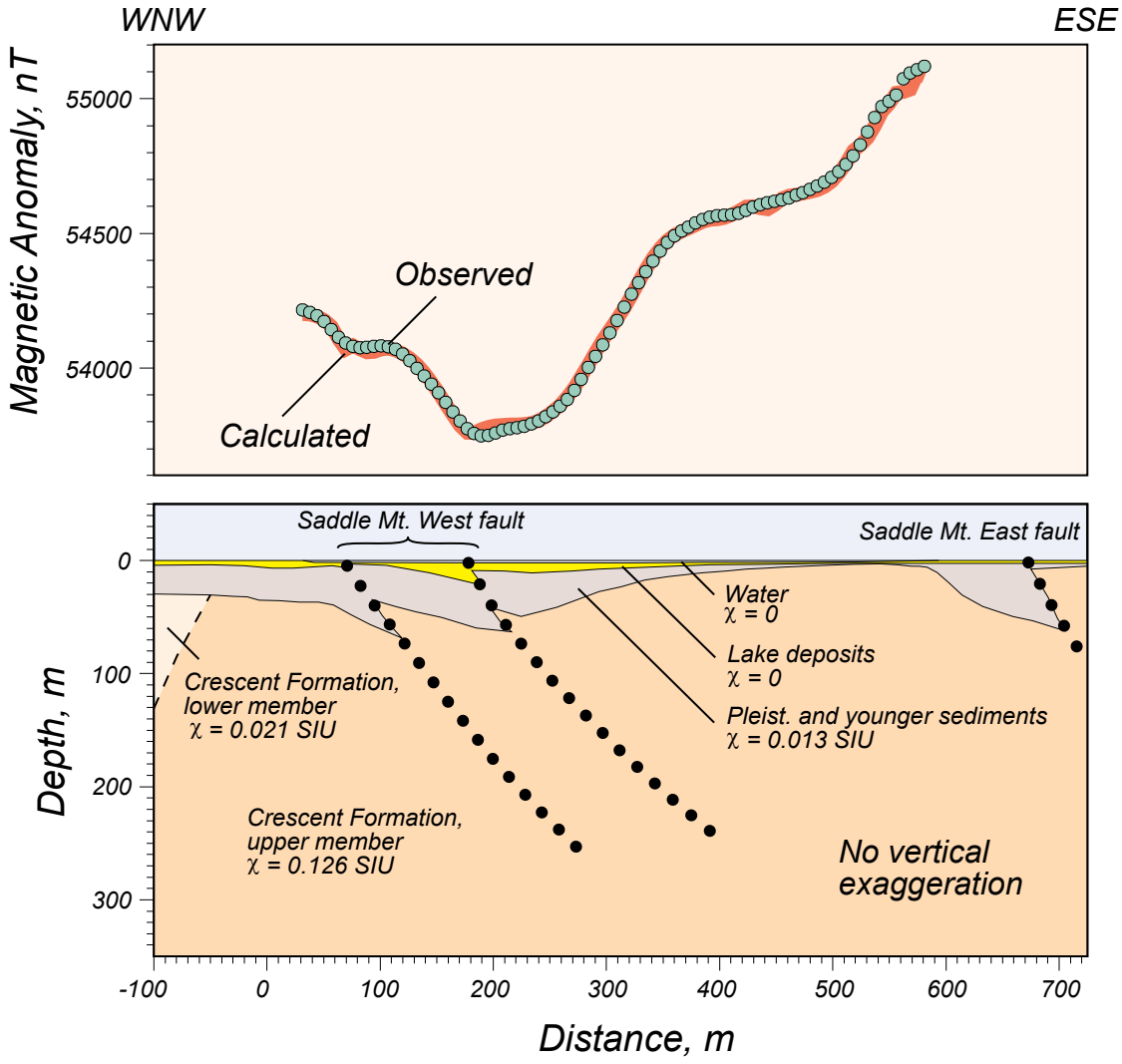
WNW
ESE
Magnetic Anomaly, nT
55000
54500
54000
Observed
Calculated
Saddle Mt. West fault
Saddle Mt. East fault
Water
χ = 0
Lake deposits
χ = 0
Pleist. and younger sediments
χ = 0.013 SIU
Crescent Formation,
lower member
χ = 0.021 SIU
Crescent Formation,
upper member
χ = 0.126 SIU
No vertical
exaggeration
Depth, m
0
100
200
300
-100
0
100
200
300
400
500
600
700
Distance, m

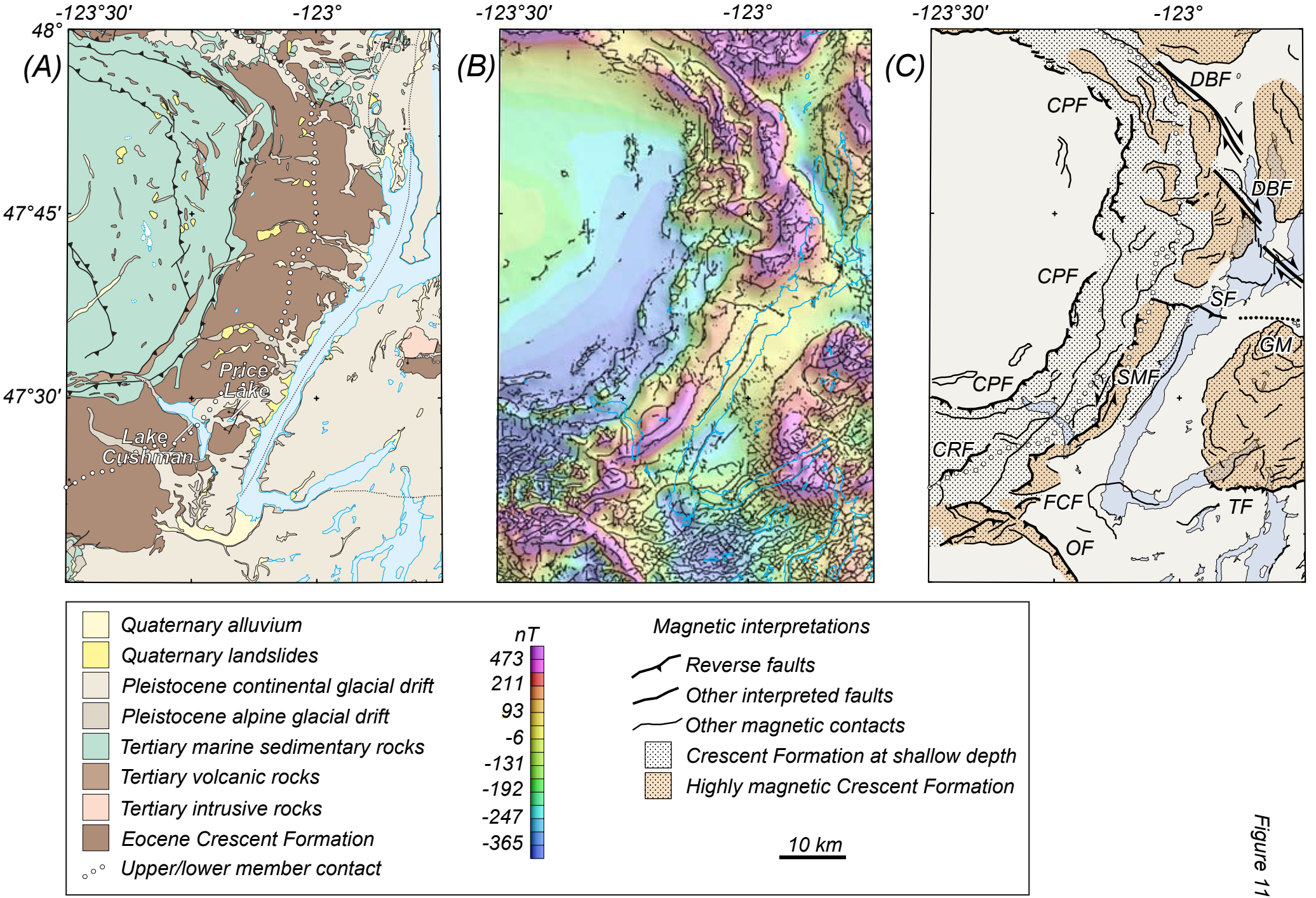
-123°30'
-123°
48°
47°45'
47°30'
(A)
(B)
(C)
Price Lake
Lake Cushman
DBF
CPF
SF
GM
SMF
CRF
FCF
TF
OF
Quaternary alluvium
Quaternary landslides
Pleistocene continental glacial drift
Pleistocene alpine glacial drift
Tertiary marine sedimentary rocks
Tertiary volcanic rocks
Tertiary intrusive rocks
Eocene Crescent Formation
Upper/lower member contact
nT
473
211
93
-6
-131
-192
-247
-365
Magnetic interpretations
Reverse faults
Other interpreted faults
Other magnetic contacts
Crescent Formation at shallow depth
Highly magnetic Crescent Formation
10 km

Figure 11

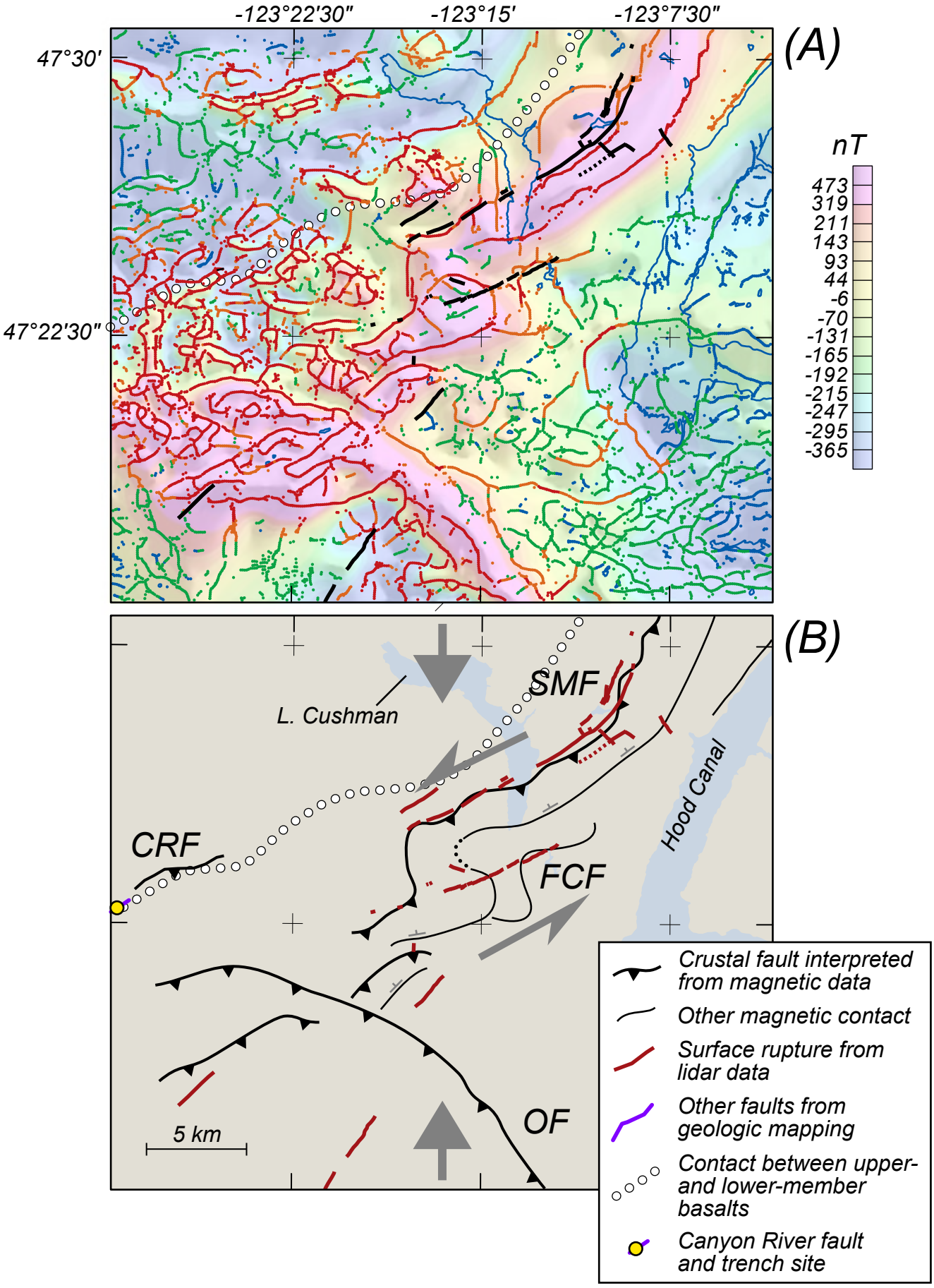
-123°22'30"
-123°15'
-123°7'30"
47°30'
47°22'30"
(A)
nT
473
319
211
143
93
44
-6
-70
-131
-165
-192
-215
-247
-295
-365
(B)
L. Cushman
SMF
CRF
FCF
Hood Canal
OF
5 km
Crustal fault interpreted from magnetic data
Other magnetic contact
Surface rupture from lidar data
Other faults from geologic mapping
Contact between upper- and lower-member basalts
Canyon River fault and trench site

Figure 13

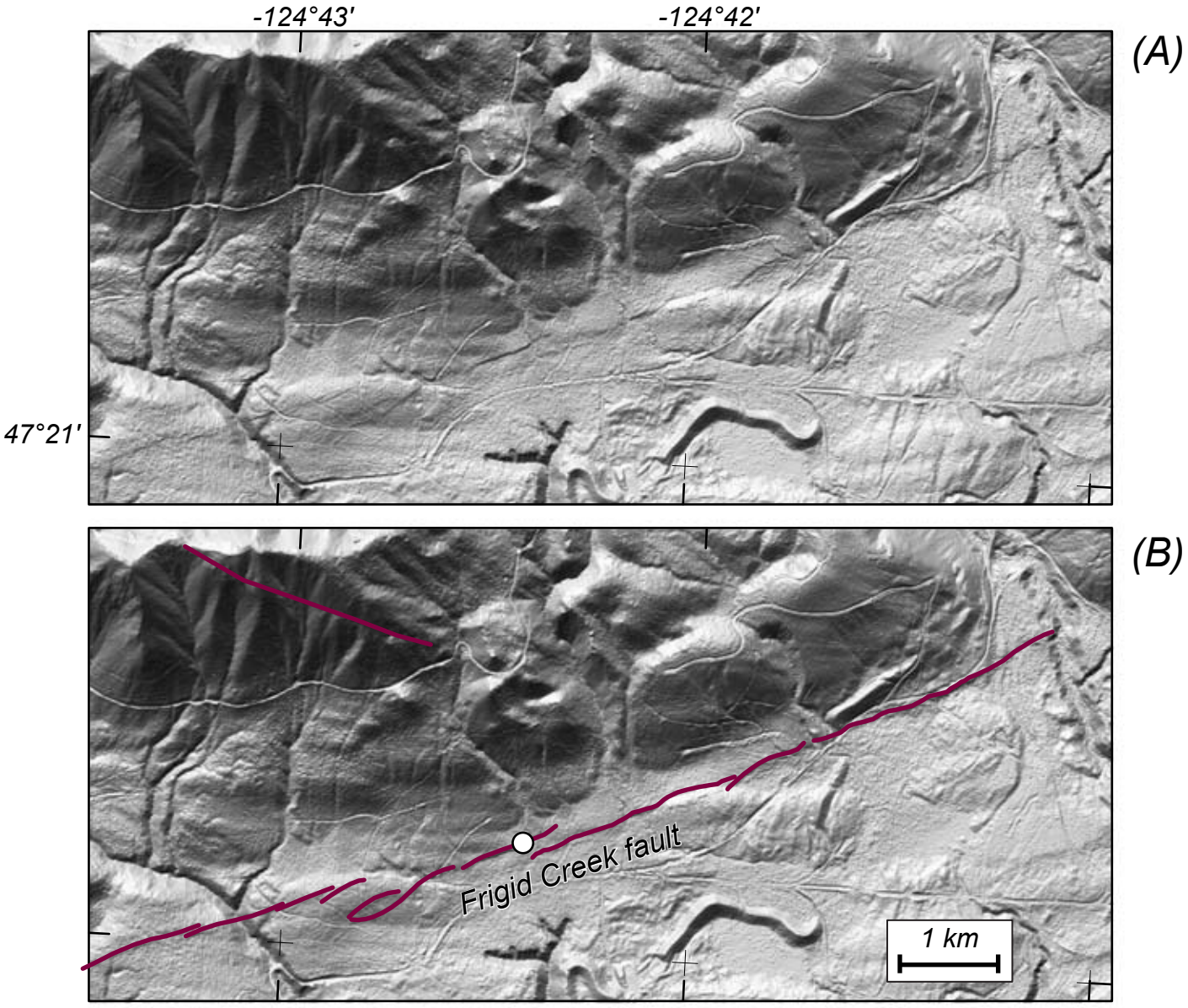

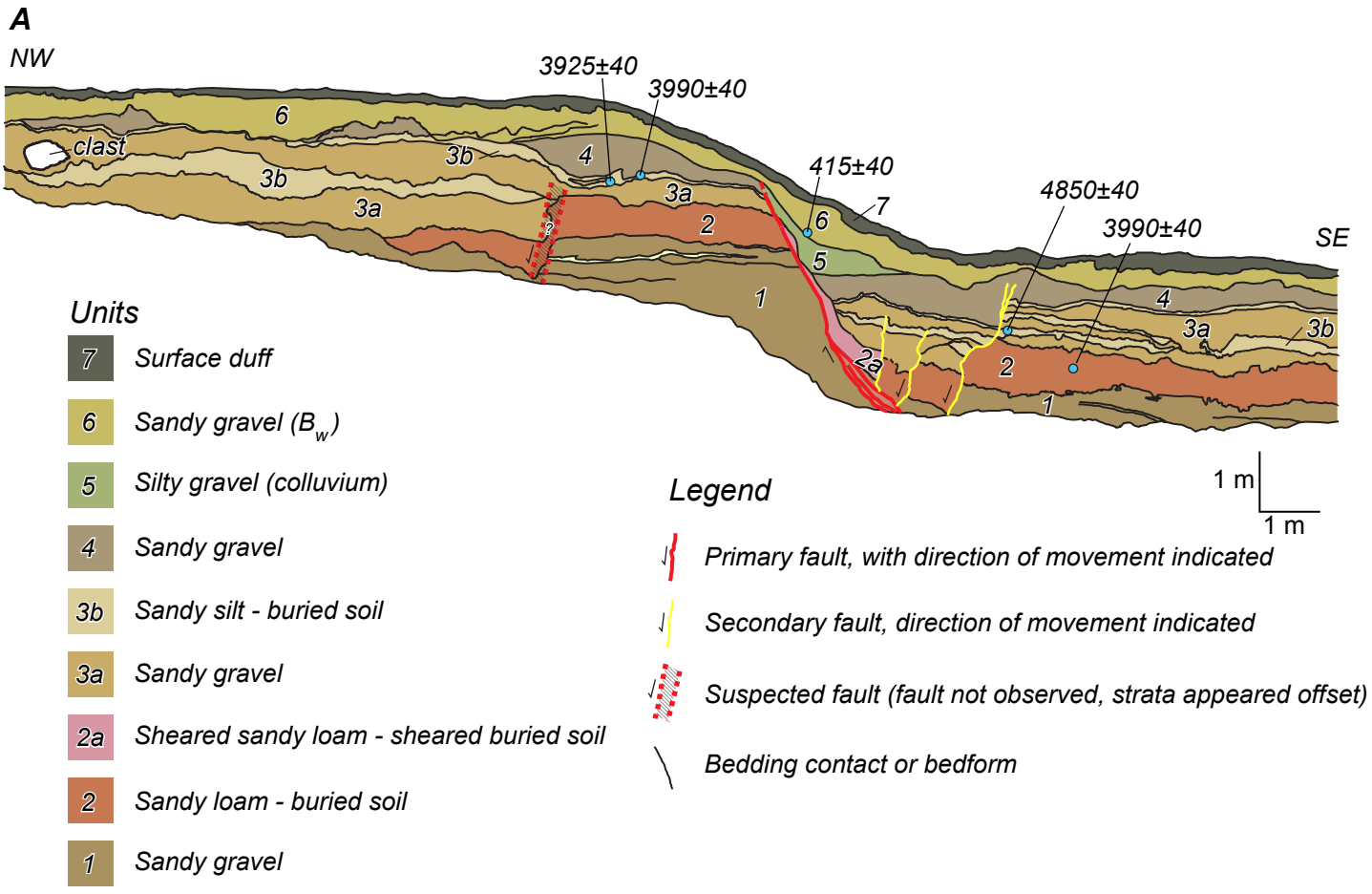
A
NW
SE
3925±40
3990±40
415±40
4850±40
3990±40
clast
6
3b
4
3a
2
5
7
1
2a
?
1 m
1 m
Units
7 Surface duff
6 Sandy gravel (B_w)
5 Silty gravel (colluvium)
4 Sandy gravel
3b Sandy silt - buried soil
3a Sandy gravel
2a Sheared sandy loam - sheared buried soil
2 Sandy loam - buried soil
1 Sandy gravel
Legend
Primary fault, with direction of movement indicated
Secondary fault, direction of movement indicated
Suspected fault (fault not observed, strata appeared offset)
Bedding contact or bedform

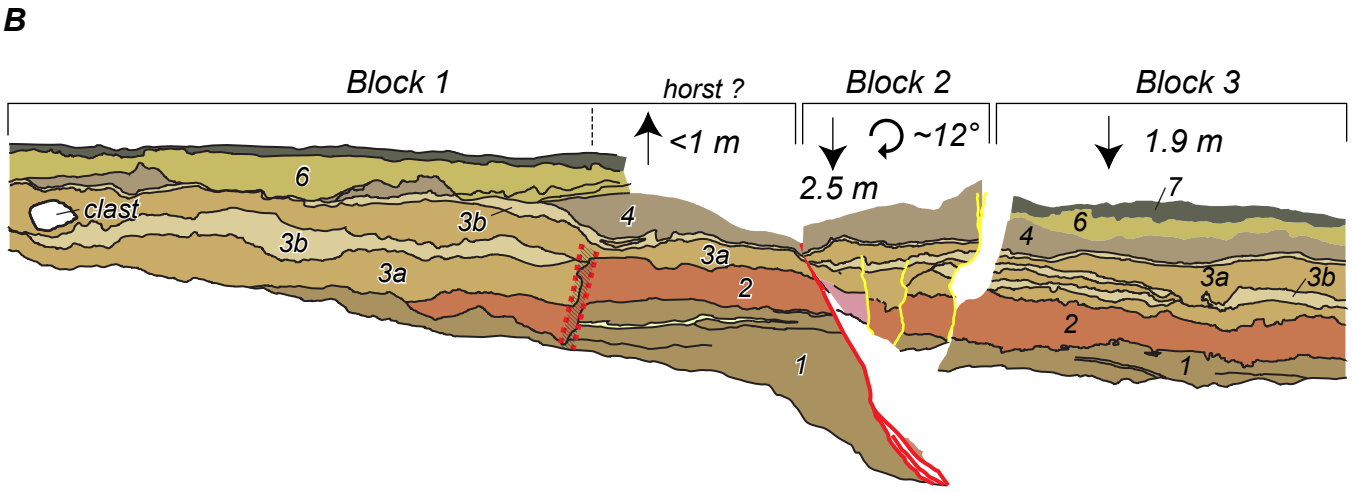
B
Block 1
horst ?
Block 2
Block 3
<1 m
~12°
2.5 m
1.9 m
clast
6
3b
4
3a
2
1
7

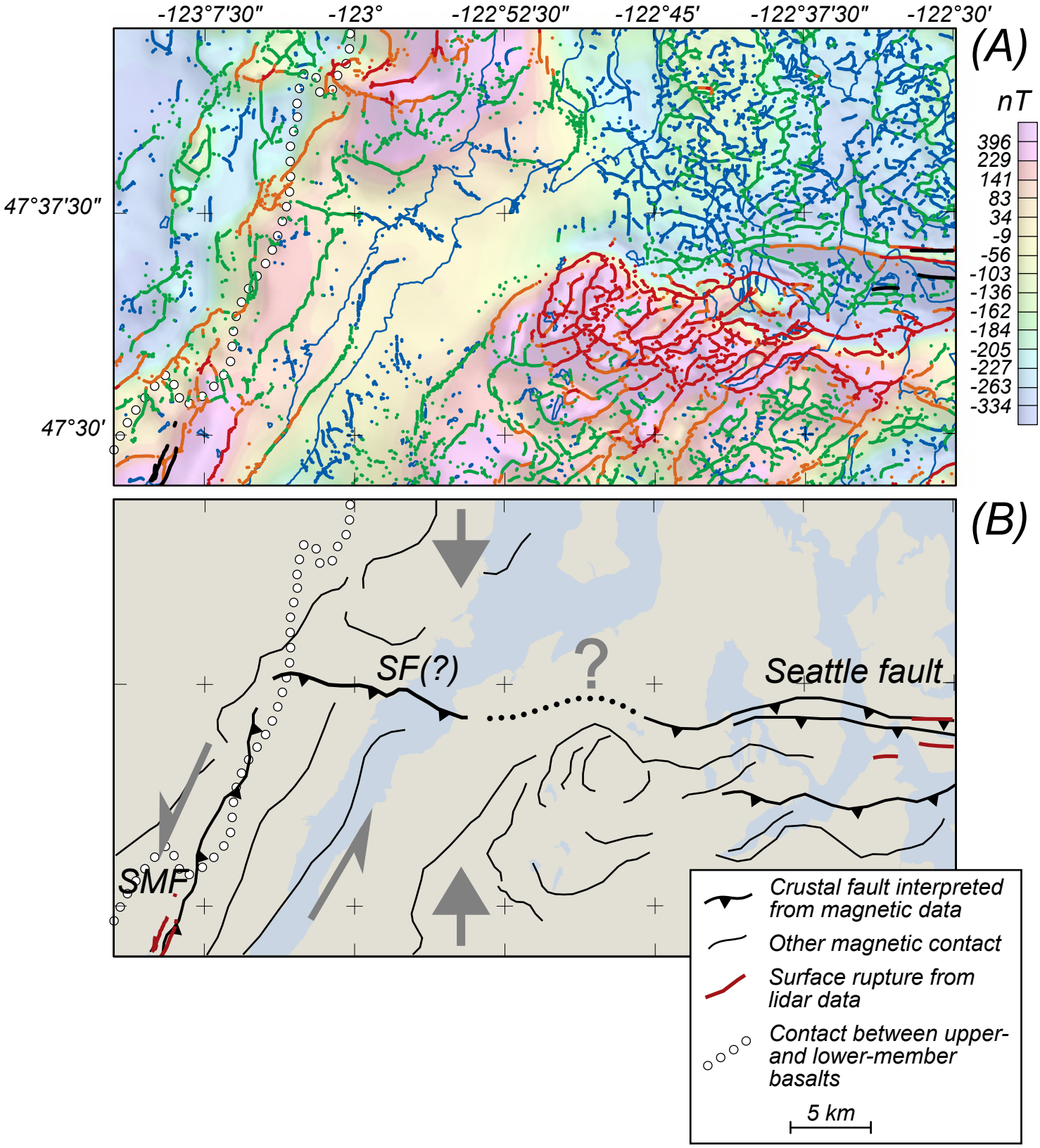
-123°7'30"
-123°
-122°52'30"
-122°45'
-122°37'30"
-122°30'
47°37'30"
47°30'
(A)
nT
396
229
141
83
34
-9
-56
-103
-136
-162
-184
-205
-227
-263
-334
(B)
SF(?)
?
Seattle fault
SMF
Crustal fault interpreted from magnetic data
Other magnetic contact
Surface rupture from lidar data
Contact between upper- and lower-member basalts
5 km

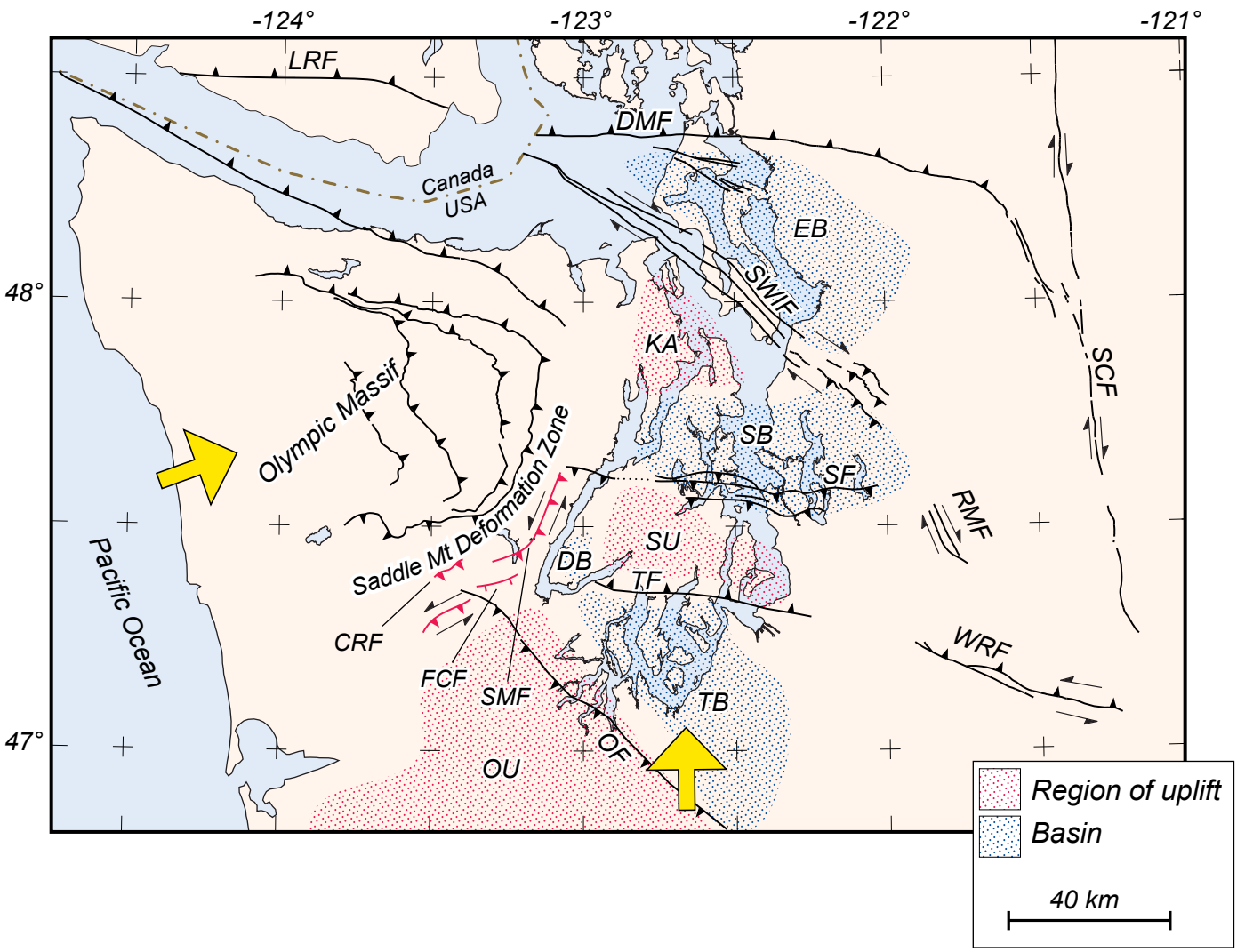
-124°
-123°
-122°
-121°
48°
47°
LRF
DMF
Canada
USA
EB
SWIF
KA
SCF
Olympic Massif
SB
SF
RMF
Saddle Mt Deformation Zone
SU
DB
TF
WRF
CRF
FCF
SMF
TB
OF
OU
Pacific Ocean
Region of uplift
Basin
40 km